Production and characterization of titanium based alloys with potential for antifouling and biofouling

A thesis

submitted in fulfilment

of the requirements for the degree

of

Masters in Engineering

at

The University of Waikato

by

Yousef Namlan Alshammari

THE UNIVERSITY OF
WAIKATO
Te Whare Wānanga o Waikato

2017

Abstract

Biofouling is the settlement and accumulation of microorganisms on the surface of a material submerged in sea water, and most of the time is an unwanted phenomenon and constitutes a financial burden. Titanium is a lightweight high strength metal characterised by good corrosion resistance, better than stainless steel, and would be the ideal material to be used in marine applications. However, biofouling would still happen in structures made out of titanium.

The aim of this study is to gain understanding of the biofouling process to be able to design Ti-based materials with the potential to prevent, or conversely enhance, biofouling, as both scenarios could have relevant industrial applications. In particular, it was planned to manufacture the Ti-based materials via powder metallurgy to take advantage of the intrinsic benefits of these techniques which include the freedom of designing new alloys, without the limits imposed by binary phase diagrams.

From literature, it was found that Cu and Mn could have respectively, the ability to reduce or promote biofouling. Therefore, various binary Ti-xCu and Ti-yMn compositions, where x = 0.5%, 2.5%, 5%, and y = 1%, 5%, 10%, were targeted and successfully manufactured via the conventional powder metallurgy route of cold uniaxial pressing plus vacuum sintering, obtaining fully homogeneous materials.

It is well known that residual porosity is still present in sintered Ti-based materials, and for that the binary Ti-xCu and Ti-yMn alloys were also a thermomechanical process via forging. This hot deformation process should reduce the amount of residual porosity, but it can also be used to tailor the microstructure, and thus the mechanical behaviour, which is paramount for many industrial applications. Along this line, it was decided to investigate the effect of the forging temperature (i.e. of the starting microfeatures) and thus forging from the β and within the α+β region was considered.

From the characterisation performed, the Ti-5Cu and Ti-5Mn alloys were chosen as the most promising alloys for the investigation of the antifouling and biofouling capability of the binary Ti-xCu and Ti-yMn alloys developed.

Acknowledgments

I wish to acknowledge and thank the following people who have been part of my educational journey and have assisted me in the writing of this thesis. First of all, to my supervisor Dr Leandro Bolzoni; my heartfelt thanks for all of your assistance and guidance. You were my inspiration and your door was always open whenever I had questions or doubts. Without the help of you, this thesis would not have been done. I consider it such an honour to have been under your supervision and guidance.

To Dr Fei Yang, Dr Stella Raynova and Dr Mingtu Jia; thank you so much for your guidance and help throughout the project, this was always delivered in a friendly and helpful manner, so I will never forget you. Also, my great thanks and best wishes to Yuanji, Chris, Shannon and Helen for all of the training and technical guidance you provided, and for the use of equipment and machines.

To my colleagues, thank you for your awesome support and motivation, it is greatly appreciated. I must also acknowledge and thank Cheryl Ward for her help in formatting this thesis.

Finally, but not least, I give thanks from the bottom of my heart to my father, mother, brothers and sister for your love and support, so freely given across the miles from Kuwait to New Zealand. I could not have done this without you. To my son, I dedicate this thesis to you and I hope that it will inspire you to achieve what you want to in life.

May God bless you all.

Table of Contents

List of Figures

List of Tables

CHAPTER 1

THE UNIVERSITY OF
WAIKATO
Te Whare Wānanga o Waikato

Introduction

Biofouling, also termed as marine biological fouling, is the unwanted accumulation of plant material, microbes, and animals on unnatural surfaces immersed in sea water [1]. Figure 1.1 shows an example of microorganism accumulated inside the wall of an industrial used pipe.

Figure 1.1 Example of fouling in the inner wall of a pipe [2].

In the context of the shipping industry, the severe effects of biological fouling include high water resistance, increased ship weight, reduction in speed and loss of maneuverability, higher consumption of fuel, higher emissions, and frequency of dry-docking. These effects arises from the roughness on ships' surfaces [3] and the increased weight of the water vessel which results in the reduction of speed maneuverability [1]. To compensate for these effects, more fuel is consumed which increases emissions. The frequency of dry-docking increases due to the extra maintenance required for the vessel. Dry-docking is expensive and removes the vessel from service for long periods. The biofouling coating formed on the vessel ultimately causes corrosion, alteration of the electrical conductivity and discoloration [1].

Lastly, as pointed out by Chambers *et al.* [3], there is also the introduction of invasive or non-native species to new environments; fouling organisms hitch hike in the ballast tanks causing adverse environmental impacts in many countries.

Biofouling has become a huge problem in the marine environment. Among the proposed solutions in the marine navigation industry, tributyltin self-polishing copolymer paints (TBT-SPC) have been identified as some of the most effective antifouls [4]. However, their usage has caused adverse effects to the environment such as the defective shell growth in oysters caused by tributyltin moiety [3]. In addition, its use has also led to the development of male characteristics in the dog-whelk female genitalia. Consequently, a ban on the use of TBT-based antifouling paints is currently in place.

Other methods such as non-toxic antifouling technology have been successfully applied, however, their usage is incapable of replacing biocide coatings [3]. For example, non-stick fouling releases compounds that do not facilitate the release of fouling organisms as anticipated. Such methods also have many drawbacks including poor mechanical properties, high costs and recoating difficulty. Other non-toxic methods, including biological methods are constrained by the sea water temperature that affects the catalytic and stability functions of enzymes [5]. Evidently, researchers are continually focusing on antifouling methods in the marine industry. Nonetheless, physical technologies could offer feasible, durable, non-toxic and effective solutions and should therefore be explored [1].

Many Ti alloys possess antibacterial properties. A combination of these properties with high specific strength, great resistance to corrosion and biocompatibility make Ti alloys excellent candidates to be used in industrial applications. Since 1940s, when the main processing technologies of Ti and Ti alloys were developed, these materials have become a great alternative to known materials, such as various super alloys based on nickel, aluminium or steel [6, 7]. At first, Ti and Ti alloys had only aerospace applications. One of the most notable early application of Ti alloys was the Lockheed SR-71 Blackbird project in the 1960s where 93% of aircraft was made from Ti alloys. In the 1970s McDonnell Douglas started to use Ti springs on the commercial aircraft DC-10. β forging was used in processing of Ti alloys in both of these cases [8]. Because of its exceptional properties, nowadays Ti is used in many other high-quality industrial applications including consumer products and biomedicine [9].

The most commonly used Ti-based biomaterials are Ti-6Al-4V ELI (or Ti-64 ELI) and commercially pure Ti. However, both materials possess disadvantages as well. The mechanical strength of pure Ti is fairly low in comparison to other available metallic biomaterials. Ti-64 ELI releases vanadium (V) and Al ions in biological environments. These two elements should be avoided because V is known for its toxicity and Al for its neurotoxic effects.

As other materials, Ti is subjected to biofouling and microbial attachment. Biofouling of heat exchangers in seawater results in the formation of biogenic MnO_2 layer on the material's surface. This process is caused by activities of manganese oxidizing bacteria (MOB). Biofilm formed as result of this process leads to decrease in heat transfer and thus lowers the efficiency of the heat exchanger. Previous studies reported that biofilm increases in time and the percentage of MOB in total count of bacteria may reach 100% in 20 months [10].

Researchers have been looking for alternative solutions for Ti-based materials used in biomedicine. On the one side, elements such as tantalum (Ta), niobium (Nb) and zirconium (Zr) have excellent biocompatibility. However, all of the listed elements are not just costly, but availability issues may arise in future. Mn is a good choice for creating biocompatible Ti alloys. It has high availability and relatively low cost. On the other side, it has been demonstrated that Cu and Ag have antibacterial properties and could be used to manufacture safer biomedical implants.

Powder metallurgy of Ti alloys has been developed and used in some of the developed countries. It has however been restricted to missile and space applications [11]. Powder metallurgy offers the possibility to design novel alloy compositions without the limits imposed by the solubility of each elements. Moreover, in the case of Ti alloys, powder metallurgy has been identified as a potential production method to reduce the final cost which is currently one of the limiting factor for the widespread use of Ti in industry.

The present work focuses on the design and manufacture of Ti based alloys to be produced via powder metallurgy techniques. The alloying elements chosen have the potential to either hinder or promote fouling; however, this initial study is focused on understanding the production of these Ti-based alloys and the properties achievable. Antibacterial and fouling experiments would then be planned on the basis of the work developed in this thesis.

Aim and objectives

Aim

The major aim of this thesis is to understand the fouling phenomenon to be able to identify alloying elements to be added to Ti with the final aim of producing Ti-based materials that can either promote or limit fouling. The study mainly addresses the production and characterisation of these novel composition to set the basis for further development in the field.

Objectives

- Review the current knowledge about fouling to be able to plan a successful way forward for the creation of Ti alloys with the potential to be applied in the marine industry;
- Design binary Ti alloys using phase diagrams and current literature;
- Prove the concept that the targeted Ti alloy compositions can be successfully fabricated using the conventional cold uniaxial pressing plus vacuum sintering route;
- Post-process the sintered alloys via forging to modify the microfeatures of the materials;
- Generate scientific understanding of the properties and behaviour of these Ti-based materials for their implementation in marine industry where antifouling or biofouling properties are needed.

CHAPTER 2

THE UNIVERSITY OF
WAIKATO
Te Whare Wānanga o Waikato

Literature review

2.1 Biofouling and antifouling

Biofouling is the undesirable accumulation of biotic components that are deposited on a surface [1, 3, 5]. In contrast to abiotic types of fouling such as particle fouling, organic and scaling fouling, biofouling is a special kind of fouling where microorganisms develop at the expense of biodegradable compounds from the water turning them into biomass and metabolic products. This can also be seen as the process of multiplication of particles by microbes [3]. Microorganisms produce extracellular polymeric substances, which keep them together and also glue them to the surface, which aggravates the fouling [12]. Biofouling is not only a threat to the technical industry, but can also represent a health hazard because the creation of biofilms by microorganisms pollutes the water and this could cause serious illness and sometimes death if the water is ingested.

In the marine context, marine fouling involves the accumulation of microbes on immersed surfaces leading to not only environmental but also economic and safety related negative consequences [3]. For instance, marine fouling generates drag resistance of vessels moving through water, consequently increasing the consumption of fuel and the emission of greenhouse gases. In addition, slime films can cause a significant increase in powering and resistance. **Figure 2.1** shows a sketch of a ship vessels where common growing areas of biofouling are highlighted.

More than 4000 species, either in sessile or attached form, and located in the shallow ends along coastal region are the primary organisms that cause marine biofouling [1, 3]. However, these are only a small proportion of known organisms, mainly because only those organisms that can adapt to the ever-changing man-made conditions can resolutely adhere to the water vessels. For example, only those organisms that can adapt to wide variations of environmental conditions such as water flow and temperature are able to dominate and are found on ship vessel as product of the fouling process.

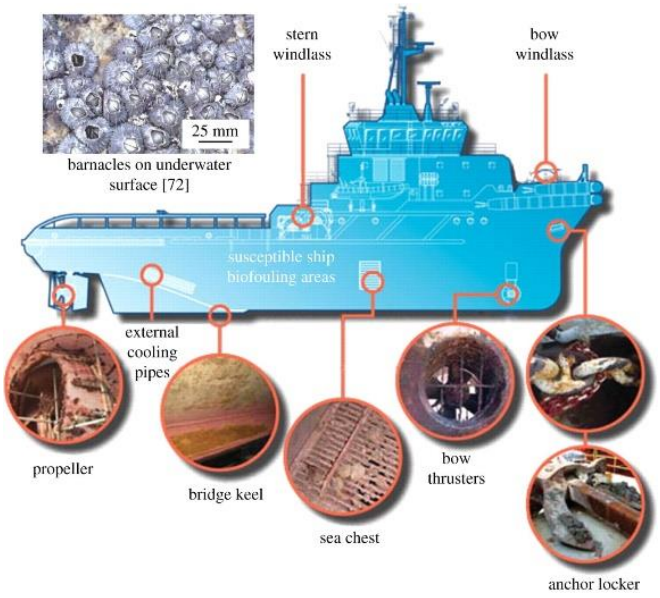

Figure 2.1 Common growing areas of biofouling on a ship vessel [13].

Conventionally, the fouling process, consists of four major steps [1]. In the first stage, following the immersion of surfaces in water, the surface adsorbs a molecular conditioning film, which is made up of dissolved organic matter. This involves the accumulation of polysaccharides, organic molecules, proteins, peptides and proteoglycans on the water vessel surface. Physical forces, including electrostatic interaction and Brownian motion, and van der Waal's force of attraction usually govern this process [1]. Unicellular organisms such as bacteria, algae and cyanobacteria colonise the surface within hours forming a biofilm (shown in Figure 2.2), which is an assemblage of attached cells also referred to as slime or micro fouling.

Figure 2.2 Biofilm accumulation in a tube [13].

These microorganisms are first adsorbed on the modified surface of the water vessel reversibly using physical forces and afterwards adhere to the surface. Other unicellular organisms such as diatoms predominate in the biofilms that adhere to certain types of antifouling coatings by secreting sticking polymeric substances by specialised body parts [1]. This type of disposition formed by the unicellular organisms provides them with protection against predators, the changing environmental conditions and toxins, and facilitates easier capture of nutrients. This is the reason why static surfaces, even those covered by biocides, eventually become coated with slime [1]. The attached cells then divide mitotically to give rise to colonies, which ultimately coalesce to form compact biofilms. The existence of polysaccharides, proteins and other adhesive exudates, and the irregular and the roughness of the microbial colonies facilitate the trapping of more organisms and particles to the colonies [1]. In some instances, macro fouling communities comprised of either hard or soft material develop and overgrow the micro foul formed by the unicellular organism. While soft fouling is made up of algae and some invertebrates such as sponges, anemones and hydroids among others, hard fouling is composed of invertebrates such as tubeworms, barnacles and mussels. The last stage entails the settlement and growth of the huge marine organism coupled with macroalgae growth.

The existence of different organisms and molecules in the film affects the settlement of successive organisms [1]. This is because they may serve as food for subsequent organisms that replace them. This may favour the discolouration and increase the surface alkalinity, which favours adhesive deposition. As found in [1], this concept may be used for the development of effective biocides to hinder this successional process during its early stages. However, this may not be easily achieved because other complex mechanisms have been described by different researchers who have expanded on the successional processes in biofouling [12]. In addition, biofouling effects depend on various parameters that include the geographic location, the water condition and vessel's operating pattern, but these factors cannot usually be modified to control the biofouling process. For instance, when it comes to temperature, which is one of the most significant measures that greatly influences the fouling process, it cannot be altered. Areas with higher temperature favour the process since they facilitate faster breeding and growth of organisms. In addition, a factor like water flow cannot be modified to reduce the process of biofouling [1].

Biofouling is one of the most costly problems in the marine industry [14]. Even though it is a common phenomenon, there is little quantitative data concerning its associated costs [15]. Based on the number of variables it is difficult to assess such costs cumulatively. Nonetheless, some authors come up with estimated costs of biofouling. For instance, organic growth increases the roughness of ships' hulls, which affects their manoeuvrability and increases drag, raising the consumption of fuel by at least 30 percent. The annual global cost of fouling in this context is therefore approximately NZ$ 4.1 billion (US$ 3 billions) [16].

Callow and Callow [14] asserted that there are also costs associated with preventive overdosing of cleaners and biocides. There is the interruption of the production process and the shortened life span of the vessels because of extended cleaning as well as the treatment of contaminated wastewater. Therefore, biofouling is one of the major challenges to the marine industry. An economically healthy antifouling industry which offers different antifouling products including biocides, cleaners, antifouling surfaces and materials among others has also to be taken into account [15]. The antifouling industry accrues billions of dollars on an annual basis considering the volumes of biocide division of some of the major chemical companies on a global perspective. Banerjee et al. [15] highlighted that the reasons for the concept include the dimensions of the problem, a variety of concerned industrial areas, and the poor efficacy of many measures of antifouling which call for frequent and ongoing control mechanisms. Corrective and preventive measures to mitigate the effects of fouling present a 10:1 to 50:1 net cost saving, depending on the type of vessel. As mentioned, authors are engaging in research to come up with cost effective strategies to mitigate biofouling associated costs [2].

Antifouling can be defined as preventing or counteracting the growth of organisms on an underwater surface [15]. In this context, it is referred to as the prevention of the growth of micro and macro organisms on the bottom side of a water vessel. The adverse effects of biofouling have been experienced for more than two thousand years. Historical records indicate that while some communities used copper (Cu) sheathing on ships' bottoms, others used asphaltum, wax or tar [1]. Some also used lead sheathed timber to prevent the growth of microorganisms such as shipworms among others. For a while, Cu was effectively used as an antifoulant until late in the 18th century, when the introduction of iron hull ships almost led to its discontinuation [17].

One of the reasons for the discontinuation was that the antifouling action of Cu was not certain and that Cu has corrosive effects on iron. Other alternatives such as zinc, lead, galvanized iron and wooden sheathing were then used. Particularly, wooden sheathing was the most preferable option since it was compatible with iron sheathing, but its use was stopped due to the high cost involved. Once again, the most important aspect of the introduction of iron ships was the renewed necessity for antifouling compositions [1].

In the mid-19th century, diverse categories of paints were introduced based on the ideal of toxicant dispersal that is exhibited in polymeric vehicles [1]. Among the most popular antifoulants were Cu oxide and mercury oxide. Binders used included turpentine oil, benzene and tar. Following the introduction of antifouling, a lot of effort was focused on finding the most effective ones. However, it was not until World War II when significant changes took place in the antifouling paint industry. These changes include the need to improve of the mechanical response of the paint and the need to deal with the rise of health concerns, which led to the discontinuation of org-no arsenicals antifoulants among others, and the introduction of sprays [1]. In the second half of the 20th century, tributyltin (TBT) was discovered by Van de Kerk and his co-workers. In the following decade, some of the significant properties of TBT were discovered and this led to its commercialisation [1]. In the mid-1960s self-polishing copolymers (SPC) coatings which incorporated TBT-based biocide were reported to have a durable effect of up to five years, with modest cost of production. However, in the early 1970s, researchers focusing on TBT found that TBT compounds had negative effects on non-target species in the marine ecosystem such as the dog-whelk and oysters due to their high toxicity and persistence [12]. Following this discovery, many governments restricted the usage of TBT-based compounds. For instance, in France, a ban was made on using TBT compounds on ships which were less than 25 meters long.

In 2001 an official ban on the use of TBT-based compounds was imposed by the International Maritime Organization and this renewed the interest in the use of Cu-based paints [3]. However, these paints also posed a significant threat to the environment [1]. Along with the increased use of these paints in the marine industry, several alternatives have also been developed, such as natural biocides and other synthetic antifoulants [18].

The worldwide costs of developing new antifouling coatings or biocides continue to escalate due to the various restrictions imposed by different governments. The increase in costs related to the usage of antifoulants paints and the intended proscriptions is now pushing for the development of new harmless approaches in the marine industry. Specifically, some of the recent developments include foul release coatings (FRCs), with low surface energy, which were initially side-lined with the introduction of TBT based coatings [1].

2.1.1 Antifouling technologies

Currently, in the antifouling coating market there are two main areas of research: chemically active coatings and non-toxic FRCs [15]. While the former inhibits or limits the settlement of marine organisms using chemically active compounds, the latter inhibits the settlement of organisms while at the same time ensuring easy removal of the settled organisms without the use of chemical reactions.

2.1.2 Biocide-based & fouling release coatings

In the case of antifouling technologies, their mode of action entails the release of active substances free from tin. According to Banerjeee et al. [15], they can be divided into three major categories: (1) soluble or controlled depletion polymer coatings, (2) contact leaching coatings, also known as hard matrix coatings, and (3) specialty polymer coatings. The main objective of the three categories is to release bioactive molecules, which are embedded in a polymer matrix, known as binder. However, the three differ from each other based on their mechanism of action, which remain partially unstated. The efficiency of biocides lasts from 12 to 90 months. These paints are usually made up of 35-50 wt. percent of copper peroxide, which functions as the main biocide, and less than 10 wt. percent of booster biocides such as Zineb, Cu pyrithione or Cu biocides. In Europe, the usage and production of non-agricultural substances for biocidal functions has been regulated to reduce the effects that are likely to arise. Therefore, when introducing antifouling paints in the markets, the manufacturing company should demonstrate the efficacy of the product and its safety [15].

As previously mentioned, FRCs are biocide-free coatings whose mode of action is based on their dual performance, including their non-stick property that limits or inhibits the adhesion of marine organisms, and the fouling release behaviour that enhances the release of marine organisms. As noted by Burgess et al. [18], coatings minimise the adhesion strength between the substrate and the fouling marine organisms comprised of barnacles among others, so that the attached organisms can be detached using cleaning mechanisms or by the hydrodynamical stress during ship movements.

As found in [4, 18] the specific fouling release properties of these compounds are related to the low energy and the surface hydrophobicity. Yebra el at. [1], however, asserted that apart from these aspects, other parameters including the roughness of the ship's surface, the components elasticity and the thickness of the film coating have an impact. Owing to their non-adhesive property, they should be applied on a tie coat, which promotes the adhesion between the anticorrosive epoxy primer and the top coat. Their reported life-time as compared to that of biocide antifouling is quite longer, typically from five to 10 years. It is important to note that this technology is not subjected to legislative restrictions yet, unlike its counterpart [1].

2.1.3 Biological methods and physical method

Some organisms can secrete metabolites and enzymes, which inhibit the growth of other organisms [19]. One major advantage is that their secretions are biodegradable and have low amounts of toxins. In recent years, biological methods have received attention, with many researchers trying to extract these secretions in high quantities to be used for biological antifouling. For instance, secretions from blue algae can undermine the diatoms' growth. Other practical antifouling agents have also been identified in organisms such as fungi, some bacteria and sponges [19]. Banerjee et al. [15] highlighted that many types of enzymes from these organisms, including transferases, isomerase, ligase and lyase have been reported to have antifouling capabilities. In the antifouling application, the enzymes are used to degrade the adhesives needed for the settlement of the organism. They are also used to disrupt the biofilm matrix and to generate biocides and deterrents. Lastly, they are used to interfere with the intercellular communication. The enzymes are used to inhibit the settlement and growth of organisms, thus are effective during the earlier stages of biofouling [3, 15].

Many physical methods have also been successfully tested for the prevention of biofouling. For instance, antifouling by radiation and electrolysis [15]. In this category, the production of hypochlorous acid (HClO), bromine and ozone bubbles through electrolysis of the sea water has been commonly used. Due to their strong oxidising ability, these compounds are spread all over the hull of the ship where they eliminate different fouling organisms. However, they are not very efficient as they induce corrosion of steel [1]. Therefore, several researchers have proposed the use of Ti supported anodic coatings due to their advantages which include low energy consumption, low decomposition tension and higher current efficiency. Other physical methods include microcosmic electrochemical methods that involve the transfer of electrons between the microbial cells and the electrode causing electrochemical addition of oxygen in the intercellular substance. Furthermore, changing the zeta potential of the surface to reduce the adherence of microbes such as bacteria has also been investigated. Finally, other methods include modification of the surface topography and the hydrophobic properties of the ship's hull. For instance, decreasing the roughness of the ship to prevent the adhesion of Pseudomonas spp. [1].

2.1.4 Alloys for antifouling or biofouling

As previously discussed, research studies such as biocide-based coatings, fouling release coatings and, physical and biological methods were targeted to prevent antifouling and biofouling. The development of novel metallic materials which can combine the structural integrity needed in the marine industry with the ability to hinder, or conversely enhance, fouling is also of practical interest. However, no much information is available in the literature and more studies are essential for the development of new alloy materials.

As previously mentioned, titanium (Ti) and its alloys would be the ideal materials because of their excellent corrosion resistance, processability, mechanical characteristics and biocompatibility. In the marine industry, the application of Ti and its alloys provides new insights for research. However, some researcher claimed that pure titanium lacks bactericidal capabilities [20] and the process of biofouling is largely enhanced by bacteria, which function as early colonisers of the substrate.

From literature it is clear that Cu have the potential of antibacterial properties which could be used to prevent fouling of submerged structures while Ti-Mn have biomineralization properties, which enhances the colonisation of bacteria, thus biofouling [21].

Regarding Cu as alloying element for Ti, it was demonstrated that Ti-Cu sintered alloy exhibited strong antibacterial properties [20]. The alloy also had significant mechanical properties including Young's Modulus, elongation and hardness. It was also resistant to corrosion. Moreover, the antibacterial effect of Ti-Cu sintered alloys were strong and stable when the Cu content of the alloy was at least 5wt. %. The antibacterial property of the Ti-Cu alloy offers promise in the prevention of earlier stages of biofouling [22, 23],

Concerning the use of Mn as alloying element, Gopal et al. [21] and Kim et al. [24] indicated that when Ti surfaces are exposed to sea water, biofilms were formed, which form the basis for attachment of various micro-organisms, corrosion and inorganic products. The studies indicated that Ti was susceptible to biofouling, since certain types of heterotrophic bacteria can oxidise manganese (Mn), a phenomenon known as biomineralization. Its inert and non-toxic nature also provides appropriate surfaces for bacterial attachment and growth. The presence of biomineralization ensures that the surfaces are nutritionally rich, and function as attractive substrates. According to Gopal *et al.* [21], these concepts provide important insights for the application of Ti.

2.2 Titanium and titanium alloy

Ti is a silver-grey transitional metal with an atomic weight of 47.90 and atomic number 22 [25]. It is lightweight and is the fourth most abundant metal on earth, making 0.62 percent. It exists as brookite, rutile, leucoxene, anatase, sphene and ilmenite. Even though it is relatively abundant, owing to the high cost of extraction, it is one of the most expensive metals available. Nonetheless, there are many applications of Ti and its alloys in the aerospace industry for aeroplane fasteners and parts [25]. It is also used in the finishing industry due to its excellent corrosion resistance and for the production of human implants, such as pacemakers and artificial hearts due to its good compatibility with the human body.

Ti was first discovered by William Gregor in 1791, however, it was named four years later after a German chemist (M. H. Klaproth) that rediscovered it [25]. Its first extraction in pure form was done in 1875 in Russia by Kirillov. It was however not until 1910 when Ti tetrachloride was reacted with sodium for the production of individual pieces of pure Ti. From the mid-1920s, following the creation of pure Ti from Ti tetraiodide through a dissociation reaction, William Kroll began investigating other extractive metallurgy methods. Consequently, these developments led to the process of isolating the mineral by reduction with magnesium, called the Kroll process, which still functions as the main process of Ti production. However, the lab process took more than a decade before industrial scale production. Ultimately, this has facilitated the use of Ti in different industries [25].

Ti has a density equivalent to 4.51 g/cm^3. Its melting and boiling points are 1668 °C and 3287 °C respectively. As mentioned previously, Ti alloys stand out because of their excellent corrosion resistance and their high specific strength. It is only starting from 300^{o}C that carbon fibre reinforced composites can beat the high specific strength of Ti and its alloys. Nonetheless, the high specific strength of Ti and its alloys at high temperatures remains an attractive property even though the maximum application temperature is limited to approximately 550^{o}C owing to oxidation. Ti alloys can compete with steel and Ni-based superalloys which have well established high temperature applications [25].

Ti crystallises into two main different structures, shown in Figure 2.3, depending on the temperature [26, 27]. At low temperatures, Ti and its alloys form alpha (α) Ti, which entails a closed hexagonal structure. Conversely, beta (β) Ti is formed at elevated temperatures, a body centred cubic structure. The β transus temperature of the pure metal is equivalent to 882±2^{o}C [25, 28].

The two crystal structures and the corresponding temperature transformation points provide bases for the metal and its alloy's unique properties. Both diffusion rates and plastic deformation are closely related to the respective crystal structures. Moreover, the hcp structures result in a distinctive anisotropy in the mechanical behaviour of Ti; the anisotropic elastic response in this case is particularly pronounced [25].

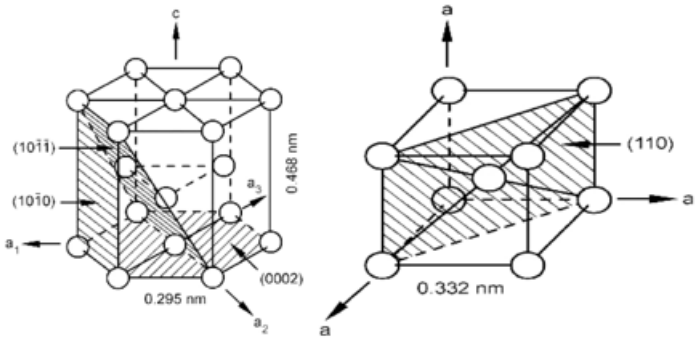

Figure 2.3 Crystal structure of Ti: a) hexagonal close packed (hcp), and b) body centred cubic structure (bcc) [25].

During the β→α phase transformation, the most densely packed bcc β planes (110) transform into basal planes (0001) of the hcp phase following the cooling of the β phase of the Ti. The distance between the (110) planes in the β is slightly smaller than that of the corresponding basal plane in the α phase [25]. Thus, the transformation of β results in a slight atomic distortion along the c-axis, which is close to the α structure a-axis. The phase transformation is also accompanied by an increase in volume [25].

Ti alloys can be classified into three different groups, including α alloy, α+β alloys and β alloys. α alloys have medium strength, reasonably good ductility, good notch toughness and desirable characteristics at cryogenic temperatures. α+β alloys on the other hand, are characterized by medium to high strengths with excellent hot forming qualities. Lastly, β alloys offers high strength up to the intermediate temperature and are readily heat treatable [29].

The alloying elements added to Ti are classified as neutral, α and β stabilisers based on their control over the β-transus temperature (Figure 2.4). While the α stabilising elements increase the α phase field to higher temperatures, the β stabilisers on the other hand, move the β phase field to lower temperatures [5, 25]. Finally, neutral elements have little effect on the β-transus temperature. Among the alpha stabilisers, Al is the only element used commercially and it is a large proportion of most major alloys of Ti as it is a highly effective α stabiliser [25]. Other interstitial elements such as nitrogen, oxygen and carbon are also α stabilisers. Another important aspect of α stabilisers is that they develop a two phase α+β field [30].

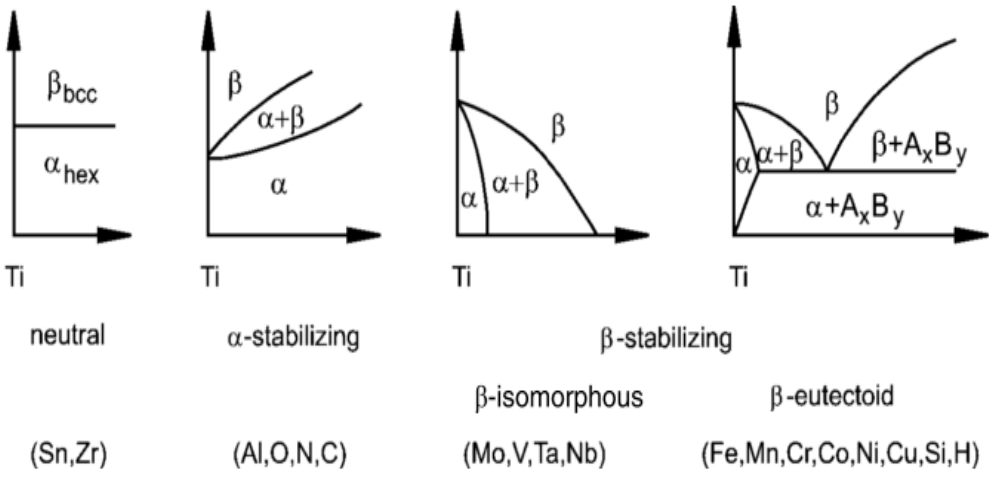

Figure 2.4 Schematic representation of the effect of different alloying elements depending on their stabilising effect [25].

At room temperature pure Ti has a stable α phase (shown in Figure 2.5), but as temperature increases the phase changes to β. For a Ti alloy containing β stabilisers, the Ti alloys phase changes to α+β or β as temperature increases, the tempereature increase required for these regions to be stable decreases with increased β stabiliser content such as Cu or Mn. Lastly, an increase in β stabilisers decreases the β-transus temperature below room temperature. After cooling however, the β phase remains stable and thus the formation of β stable alloys [30].

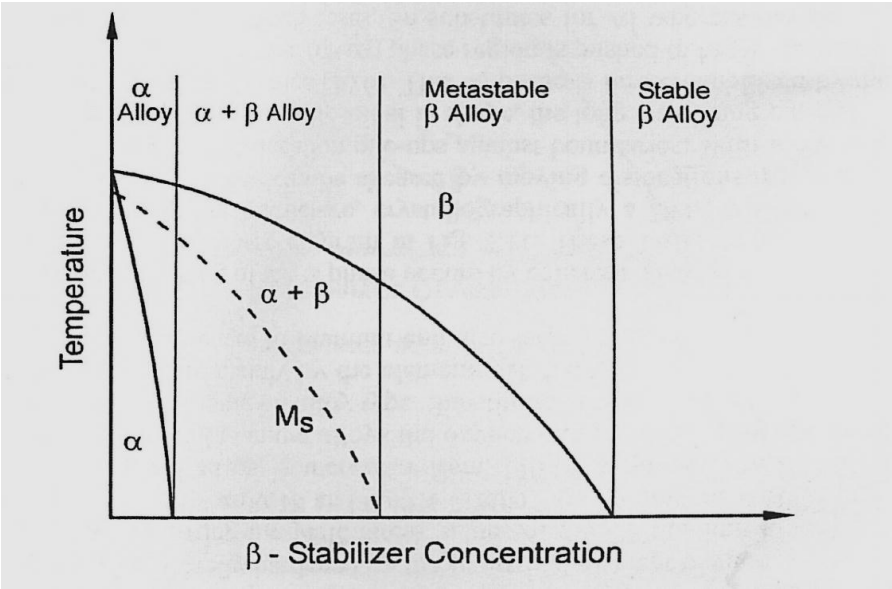

Figure 2.5 Classification of Ti alloy on the basis of pseudo-binary phase diagram [25].

2.2.1 Processing of titanium and its alloys

There are two main methods that can be used to fabricate not-easy-to-machine materials and they are powder metallurgy and casting. Both these methods have met several challenges when considered for the production of Ti. The two are related as they are the only alternative to fabricate metallic products whose shape and size is not economically achievable using traditional methods. For Ti, these practices have been extensively studied, however, the commercial exploitation of the developmental work performed is still little [26]. For instance, the refractory materials commonly used in foundries are severely attacked by Ti making it difficult to obtain a sound casting. In the case of powder metallurgy, the early Ti powders available lacked sufficient purity for the production of ductile metal compacts [26]. However, powder metallurgy has the potential to be used to easily obtain complex geometry parts made out of Ti alloys.

Powder metallurgy

Generally, the production of Ti in powder metallurgy entails production, processing and fine particle consolidation to produce a solid material. Furthermore, the homogenous and small powder particles result in a uniform final production. The Ti powder metallurgy is divided into two approaches: blending elemental and prealloying. In the blending elemental approach, the small regular powder particles, which are rejected during the ore conversion, are used as the starting points [11]. Alloying elements are added either via individual chemical elements or via master alloys. The blended mixture is then compacted with a pressure of 400 MPa to obtain a density of about 90 percent [31]. The process can be carried out using a simple mechanical press or isostatic (referred to as CIP). It is then sintered to increase the density and form chemical homogenisation. For a further increase in density, the bulk can be taken through hot isostatic pressing (HIP). The HIP hot and cold isostatic are referred to as CHIP. When using elastomeric moulds, the CHIP technique can produce complex shares which are unfeasible using the forging method [29]. The consolidation process of pre-alloyed powders can be accomplished using any known powder metallurgy procedure. After consolidation, the formed article may be subjected to an annealing heat treatment, which is carried out between 20 to 30 percent of the β transus temperature of the alloy for about two to 36 hours in an inert environment or vacuum to prevent oxidation.

Thermomechanical processing

The usual Ti alloy processing route consists of different steps: mixing of Ti sponge and master alloys, pressing this mix to briquettes, manufacturing of electrodes, double or triple vacuum arc remelting (VAR), primary processing operations such as breakdown forging of received ingots, secondary processing operations like forging. Forging is the most commonly used secondary processing route because it permits to tailor the microstructure and the properties.

The main advantage of thermomechanical processing is the ability to control the properties of the final product. By changing the chemical composition of the material and the processing conditions it is possible to obtain material suitable for specific applications. Thermomechanical processes are well developed but in the case of Ti a narrow processing window in comparison to alternative materials, primary steel and aluminium alloys can only be used due to the very high flow stresses of Ti alloys during thermomechanical processing. As such, the required working pressure is much greater than during processing of steel and aluminium. More than that, the hot workability of most of Ti alloys greatly depends on temperature decrease. Because of these reasons, it is usually hard to apply net- or near-net-shape processing [32]. Although it should be noted that such approach became possible in recent years if near-isothermal or isothermal metalworking methods are used [33, 34]. Thermomechanical processes require expensive heavy-weight press equipment that needs a lot of space and few facilities area available around the world [35].

The primary thermomechanical processing (i.e. breakdown forging operation) usually starts on forging press with a temperature approximately 150°C above the β transus temperature. There are two types of breakdown forging operations usually used during primary processing: cogging and upsetting. Cogging is a process where sides of the round ingot are pressed incrementally between flat dies. Then the ingot is rotated and moved forward. As result of this operation, a long billet with small diameter is created. Upsetting is a process where the ingot is compressed between flat dies along its axis. This operation may be used prior to cogging to grant additional deformation [32]. The temperature of the final reduction during breakdown forging operations is carefully controlled to keep it below the β transus

temperature. This is related to the ingot's heat loses during the breakdown processing thought contacts with the dies and from radiation [35].

In secondary thermomechanical processing, Ti mill products produced as result of breakdown forging operations need to be shaped into actual component. This part is done by mechanical deformation operations that can create rough shape material with the required properties. There are two main types of such operations: ring rolling and forging. Other types of deformation operations are used as well, such as extrusion and compression [36]. However, applications of these methods are much less common than forging or rolling. Specifically, the principal shaping process used for Ti alloy components' production is forging. There are two methods: open die method and closed die method. The forging die constrains the work piece in a closed die forging while there is no such die on an open die forging. Boundary conditions required for these two forging methods are different. Although the closed die process is quite harder to model, it is much easier to control [37]. Choice of the forging method depends on not just the needed degree of control over microstructures but economic factors must be considered as well.

Forging has a significant effect on the microstructures and mechanical properties of Ti alloy [32]. The final properties and microstructures of the Ti alloys depend on the chemical composition, process temperature (relative to the β transus temperature), thermomechanical processing conditions and heat treatment. Key parameters that influence the microstructure and properties of the alloy and should be carefully considered are: temperature, dwell time, deformation rate, deformation degree and cooling rate after forging. The forging temperature affects workability, type of formed microstructures and grain coarsening (if the temperature is higher than the β transus temperature). The dwell time influences interstitials pickup such as hydrogen and coarsening of microstructures (especially if the temperature is higher than the β transus temperature). The degree of deformation influences the workability of the alloy, the microstructures as well as recrystallization and kinetic heating during deformation. The cooling rate after forging influences precipitation and transformation behaviours of the Ti alloys. Graphic interpretation of dependence of temperature from time. The effect of the forging processing parameters is schematically shown in **Figure 2.6**.

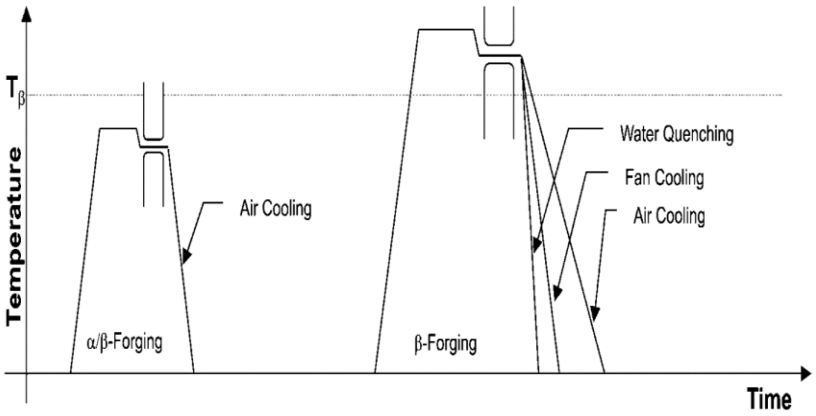

Figure 2.6 Parameters influencing forging of Ti alloys [6].

The α and β phases have specific plastic and elastic properties. Commercial α+β alloys usually have from 10% to 20% β phases at room temperature. As rule, near-α alloy have less than 10% β phase. It should be noted that approach to forging is similar for near-α alloys and α+β alloys because of similar microstructure controlling methods.

α+β forging

α+β forging is the most commonly used type of secondary thermomechanical processing method. During this process, the alloy is heated to temperature from 30ºC to 100ºC below the β transus temperature. Such high temperature is required to obtain crack-free forging if the degree of deformation is high. To avoid microstructure overheating the temperature should not exceed the β transus temperature. The ductility of forged Ti alloys increases with increasing cooling rate, however at some point it reaches its maximum value and then declines. Fracture via ductile transcrystalline dimple type occurs at low cooling rates and fracture via ductile intercrystalline dimple type may be observed at high cooling rates. It should be noted that the effect of having a continuous α layers on mechanical properties and particularly on ductility is much more apparent for high strength β alloys. This may be explained by the higher strength difference between α layer regions and matrix in β alloys in comparison to α+β alloys. After α+β forging the Ti alloy is air cooled [6]. α+β forging allows to obtain microstructures of three different types: fully equiaxed structures, fully lamellar structures and bi-modal (duplex) microstructures.

Lamellar microstructures are characterized by lower strength, lower formability, and better low-cycle fatigue performance in comparison with other microstructures that is possible to obtain in α+β forged alloy [35]. Lamellar microstructures can be formed in the finishing steps of the thermomechanical processing route by using heat treatments such as recrystallization annealing. For this reason, it may be called "β annealed" microstructure. The β grain size of such microstructure is usually approximately 600 μm. Typical width is in range of 0.5-5 mm and length could be hundreds of mm. The key parameter that affect the formation of this microstructure is the cooling after the recrystallization heat treatment where higher cooling results in finer lamellas.

Bi-modal or duplex microstructures consists of lamellar structures and equiaxed α. Bi-modal microstructures can be obtained by annealing in the α+β field if the temperature is barely below the β transus temperature. In bi-modal microstructures the size of α colony is much smaller (approximately about the size of β grain) than the size of α colony in lamellar microstructures. As such, in comparison to lamellar microstructures, bi-modal microstructures show better mechanical properties, such as higher high-cycle fatigue strength, higher low-cycle fatigue strength, higher ductility and slower fatigue crack propagation rate of microcracks [35]. Another parameter that influence mechanical properties of this microstructure is the partitioning effect of alloy element.

Fully equiaxed microstructures consist of equiaxed particles of primary α phase and β-phase that is located along the boundaries of grains. Such microstructures can be formed using same the method as bi-modal microstructures. However, it should be noted that to get fully equiaxed microstructures that have small sizes of α grains a fast cooling rate from the β phase field is needed after recrystallization. Its mechanical properties depend on size of α grains and it is possible to achieve small grains [35]. The mechanical properties of this type of microstructure are mainly influenced by the size of α grain. High values of high-cycle fatigue strength can be achieved, values that are higher than of lamellar microstructures (although lower than of bi-modal microstructures). The ductility of fully equiaxed microstructures is usually very high too, it may be even higher than of bi-modal microstructures. Value of low-cycle fatigue strength is lower than of bi-modal microstructures.

β forging

β-forging is a less commonly used type of thermomechanical processing. However, such approach has been found the most suitable for a range of modern Ti alloys. Unlike α+β alloys, β alloys cannot be transformed martensitically when quenched. As result, metastable β phase is formed. It is possible to precipitate α phase as platelets that have high volume fraction. As such, the key characteristic of any β alloy is that it is possible to harden such compounds to higher yield stress levels in comparison to α+β alloys. There is another major advantage of such alloys, it is possible to process them at much lower temperatures. Some β alloys may be even cold deformed. The corrosion resistance of β alloys is not worse, and in some cases even better than corrosion resistance of α+β alloys [32].

During β-forging Widmanstätten microstructures may be obtained. Such microstructures are also called acicular alpha microstructures. Microstructures of this type may enhance some properties such as resistance against fatigue-crack-propagation, toughness, and creep resistance. The losses in ductility and strength are relatively moderate. In order to get this attractive combination of properties, partially unrecrystallized beta grain macrostructures must be obtained by using large reductions in the β-field [35].

Heat treatments

Heat treatment techniques are used following α+β forging. Heat treatment allows to achieve the final desired properties in Ti alloys. As with forging, there are α+β heat treatment processes and β heat treatment processes. The main heat treatment processes are: solution heat treatment and aging, duplex annealing, beta annealing, recrystallization annealing, mill annealing and beta quenching.

Solution heat treatment and aging is a process where an alloy is treated at approximately 40 ºC below the β transus temperature then water quenched. After that, it is aged for 2-8 hours at temperature of 535-675°C to improve the strength. As result of this heat treatment, either α and tempered α` microstructures are formed or a mixture of α+β microstructures. The fineness of the structures depends on the temperature during the solution heat treatment and the rate of cooling. Duplex anneal is a process the alloy is treated at 50-75 ºC below the β transus temperature then air cooled followed by aging for 2-8 hours at temperature of 540-675°C. As result, primary α and Widmanstätten α+β regions are formed. Widmanstätten

microstructure grants lower ductility and increased fracture toughness [6]. In beta annealing the alloy is treated at approximately 15ºC below the β transus temperature then air cooled. After that it is stabilized for 2 hours at temperature of 650-750°C. As a result, Widmanstätten α+β colony microstructures are formed.

Recrystallization anneal is a process where Ti alloys are kept for 4 hours at temperature of 925 ºC prior to cooling at 50ºC/h to 760 ºC plus final air cooled. As result of this process, equiaxed α with β at grain-boundary triple points microstructures are formed. Mill anneal consists of α+β hot working following annealing at 705 ºC. The process lasts from 30 minutes to several hours. Then alloy is air cooled. As result, incompletely recrystallized α with a small volume fraction of small β particles microstructures are formed. Beta quenching is a process where the alloy is treated at approximately 15ºC below the β transus temperature then water quenched. After that it is tempered for 2 hours at temperature of 650-760°C. As result, tempered α` microstructures are formed [32].

There are many experimental works and research papers about the effect of different heat treatment methods on different Ti alloys. Effect of solution heat treatment and aging on Ti-Cu alloys were studied by Holden group back in 1955 [38]. Solution heat treatment on the Ti-10V-2Fe-3Al alloy is described in work by Srinivasu and co-workers. Scientists found out that α+β solution heat treatment that follows α+β rolling gives superior tensile properties. A+β solution heat treatment that follows β rolling resulted in greater fracture toughness [39]. Annealing of two Ti-Mn alloys (Ti-1.8Mn and Ti-0.4Mn) was studied by Singh and Schwarzer. Lamellar, Widmanstätten and equiaxed microstructures were produced [36].

2.3 Titanium alloys targeting antifouling and biofouling

2.3.1 Ti-Cu alloys

Alloys of Ti have been widely used in various biomedical applications such as materials for bone implants (bone screws, bone plates) and dental implants. Although conventional Ti alloys have great corrosion resistance, biocompatibility and mechanical properties, these material possess some disadvantages as well. Using traditional Ti-based materials often lead to bacterial infection that may result in implantation failure. One of the solutions for this is using an antibiotic or create implants made of materials that have superior antibacterial properties [40].

Ti-Cu alloys are one of possible candidates for biomedical application. The Cu content of the alloy improves both mechanical properties and the final antibacterial activity of the material [41]. Related studies shows that the Cu content and Ti_2Cu precipitation determines the antibacterial properties of the material [42]. Ti-Cu alloys produced by sintering method exhibit great biocompatibility, on par with pure Ti. More than that, experiments with MG63 cell line shows that the increase in the Cu content does not affect morphology of cells, cell viability or differentiation of cells [43].

Many researches indicate that Ti-Cu alloys exhibit good antibacterial activity against E. coli and S. aureus. However, to produce material with strong antibacterial properties against these bacteria, the content of Cu should be at least 5wt.%. Liu *et al.* proposed that this may be explained by release of Cu ions as result of the galvanic corrosion between Ti matrix and Cu phase [41]. In another work by the same researcher, it was stated that the release concentration of Cu ions should be in range 0.69-0.83 mg/l [44]. Various surface treatment techniques can be used to improve biocompatibility of Ti-Cu alloys such as: sandblasting, alkaline heat treatment and sandblasted and large-grits acid etching. Heat treatment methods are also able to significantly improve antibacterial properties [45].

2.3.2 The effect of addition of Cu in Ti-Cu alloys

The Cu content in Ti-Cu alloys affects the melting point of the material where a higher Cu content leads to lower melting temperature. The concentration of the alloying element also influences the mechanical properties of each Ti-Cu alloy. The density of the alloys increase linearly with an increase of the Cu content [46]. The yield strength of the material surges until 5 wt. % Cu following by its gradual decrease at higher Cu concentration [41]. With the increase of the Cu content, the UTS of the materials increases. This may be observed even if the concentration of Cu is just 0.5 wt. %. On the other hand, the compressive strength of alloys decrease at higher Cu content [41]. It should be noted that values of the hardness and Young's modulus of different Ti-Cu alloys are almost the same with only slight increase at higher wt.% Cu [41, 46]. Higher Cu content results in better grindability of the alloy [47].

2.3.3 Production methods of Ti-Cu alloys

Arc melting

Experimental Ti-Cu alloys are prepared by arc melting on a water-cooled Cu hearth. This procedure is done under argon atmosphere of high purity by using tungsten electrodes. The material is remelted 5 to 7 times to achieve homogeneity of the alloy sample (to eliminate the segregation). Kikuchi *et al.* in their work used this method to produce binary Ti alloys with Cu (5, 10, 20 and 30 wt.%) [46]. In another work by Kikuchi *et al.*, argon-arc melting method was employed to produce another set of Ti-Cu alloys with the alloying element content 0.5, 1.0, 2.0, 5.0 and 10 wt.%. Sponge Ti (purity of 99.8% and higher) and pure oxygen-free Cu pieces (purity of 99.99% and higher) were melted into 30 g buttons. Then these buttons were remelted and cast into a magnesia mould using centrifugal casting machine [48]. A similar technique was described in a work by Takahashi *et al.*, in which a dental casting unit was used for casting of Ti-Cu alloys (from 2 to 10 wt. % Cu) [47]. Hayama *et al.* produced samples of Ti-Cu alloys with the Cu content 5.0, 7.1 and 15.0 wt. % using arc melting. Grade 2 Ti and Cu with high purity (99.99%) were used as raw materials. Some of alloy samples were further heat treaded using solution treatment and furnace cooling [49]. Wang *et al.* also described a similar method for the production of Ti-5Cu alloy, but after remelting for five times they hot forged the ingot at 900 °C [50]. Zhang *et al.* used arc melting method to fabricate samples of Ti-Cu alloys with 2, 3 and 4 wt. % of alloying element. After remelting process, the ingots were solid solution treated (900°C, 3 hours) and later underwent ageing treatment (400°C, 12 hours) [45].

Powder metallurgy

Hot pressure sintering

In this method, raw materials (high purity Ti and Cu powders - 99.99 wt. %) are ball milled for 3 to 6 hours. Then, the mixture is hot sintered into samples for 3 to 6 hours under vacuum conditions within a pressure range of 5 to 35 MPa and temperature range of 850 to 1080 °C. Zhang *et al.* reported that they produce various Ti-Cu alloys using hot pressure sintering method: Ti-10Cu [40, 44, 51]; Ti-2Cu, Ti-5Cu, Ti-10Cu and Ti-25Cu [43]. Liu *et al.* also applied this method to obtain Ti-Cu alloys with the Cu content 2, 5, 10 and 25 wt. % [41].

Pressureless sintering

Another powder metallurgy technique that is used in fabrication of Ti-Cu alloys is pressureless sintering process. High purity Ti and Cu powders are mixed, and then mechanically alloyed using a planetary ball mill (rotation speed of 300 rpm). Process is done under an argon atmosphere. Stearic acid can be added to the mixture as process control agent (0.5 wt. %). Then the resulted mixture undergoes uniaxial cold pressing (pressure ~ 1GPa). The final step is pressureless sintering (850 °C, 2 hours). Similar method was also applied by Akbarpour and Javadhesari to fabricate samples of equimolar Ti-Cu alloys [52].

Laser surface alloying technique

The laser surface alloying technique is a non-conventional method of obtaining samples of Ti with alloying layers on the surface. In the method [53], pure Ti (Grade 2) was used as substrate and Cu powder as alloying material. Slurry of Cu and acetone was applied on the Ti. Ytterbium fiber laser (1.07 μm wavelength) was used to produce linear laser track of the material's surface. The laser power varied from 200 to 400 W. To inhibit oxidation of the melting area, a protective flux of argon (30 l/min) was used.

Semi-solid forging

Another technique proposed by Yongnan *et al.* was semi-solid forging method. This method was used for secondary processing of Ti-Cu alloys. Such forging process require lower upsetting forces than conventional solid forging. The temperature used in this process was 1000-1150°C. It was shown that Ti-Cu alloys forged by this method has great workability and forging ratio up to 75% [54].

2.3.4 Properties of Ti-Cu alloys

The densities of Ti-Cu alloys are much higher than of pure Ti [46]. In case of the sintered Ti-Cu alloys, the relative density is approximately 97% of the theoretical density that means that there are pores in the materials. As a result, these alloys are less ductile than pure Ti due to the presence of the residual porosity or the presence of the Ti_2Cu phase [42]. As reported by the literature, hot forming processing methods such as extrusion can improve the ductile properties [55]. To produce fully dense alloy, some densification processes should be applied such as forging or extrusion [40].

The ultimate tensile strength (UTS) of Ti-Cu alloys is greater than of pure Ti (434 MPa for Grade 1), but lower than for Ti-64 ELI (1000 MPa). It should be noted that substantial increase in strength was observed in Ti-5Cu and Ti-10Cu alloys that have hypo- and hyper-eutectoid structure [48]. Solution treatment and aging treatment can increase the strength of Ti-Cu alloy even further, unlike annealing [56]. The highest UTS value for Ti-Cu alloy is about ~900 MPa for heat treated samples of alloys with low concentration of Cu (~5-7%) [49]. The Young's modulus of Ti-Cu alloys is also higher than of pure Ti (~112 GPa) and Ti-64 ELI (116-120 GPa) and it may reach 134 GPa [46]. By using the laser surface alloying technique, it is possible to improve the Young's modulus (almost up to ~155-160 GPa depending on distance from surface).

Ti-Cu alloys possess higher hardness than pure Ti (165 HV) and higher than Ti-64 ELI (325 HV). It is explained by homogeneous distribution and good precipitation of Ti_2Cu [42]. The hardness of Ti-Cu alloys can reach up to 396.5 HV (twice then pure Ti value) [40]. Literature reports that additional processing techniques such as hot extrusion [55] or laser surface alloying technique [53] could even further increase hardness values. All Ti-Cu alloys display a much higher compressive strength than pure Ti. Such alloys can exhibit compressive strength up to 1707 MPa [44].

Ti-Cu alloys have slightly less corrosion resistance than pure Ti [41]. However, corrosion properties can be improved by T4 and T6 heat treatments [42]. These properties may also be significantly enhanced during hot extrusion [55]. The addition of Cu may increase the poor tribological characteristics of pure Ti such as wear characteristics and resistance to plastic deformation. These properties are vital in biomedical applications [57]. In comparison to pure Ti, Ti-Cu alloys show lower friction coefficient and higher wear resistance values [52]. The grindability of Ti-Cu alloy is 2.9 times higher than of pure Ti (1500 m/min) [47].

2.3.5 Ti-Mn alloys

Santos *et al.* studied the antibacterial properties of four Ti-Mn alloys with different content of Mn - Ti-6Mn/Ti-9Mn/Ti-13Mn/Ti-18Mn (6, 9, 13, 18 wt. % respectively) [58]. An immersion test using SBF (simulated body fluids) was done to investigate the biocompatibility of the materials. During the test, each Ti-Mn

alloy exhibited its own consistent ion release rate. Antibacterial properties of alloys can be explained by the ability of Ti-Mn alloys to form the oxide layer. SBF test also indicated that the oxide layer of Ti-Mn alloys has an ability to reform thus preventing the excessive release of Mn ions. The ANOVA (analysis of variance) test indicated that if the content of Mn in the alloy is higher than 13%, it may lead to Mn intoxication. After 72 h incubation period, test shows large areas of Ti-18Mn material uncovered by oxide layer. At the same time, counting of the living cells in tests with Ti-6Mn, Ti-9Mn and Ti-13Mn shows no significant difference. As such, this research suggests that Ti-6Mn, Ti-9Mn and Ti-13Mn have excellent cell proliferations and Mn can be used to produce good biocompatible alloys. However, it was recommended to avoid using Ti-18Mn in biomedicine applications because of risks of Mn intoxication [58].

2.3.6 The effect of addition of Mn in Ti-Mn alloys

The content of Mn in Ti-Mn alloys affects the mechanical properties and the microstructures of the material. With the increase of the Mn content the α-Ti phase proportion decreases, but the precipitation of β-Ti phase increases. The Mn content positively shifts the electrochemical potential of the material. It means that higher Mn content leads to better corrosion resistance of the alloy. This may be explained by the enhanced cathodic reaction that promotes the active-passive transition [24]. The content of Mn also affects antibacterial properties of Ti-Mn alloys. Higher amount of Mn in alloy leads to smaller cell proliferation [58].

Mn is an element that has good solid solution strengthening capacity. That is why with the increase of the Mn content the Vickers hardness of the alloy also increases. However, with increased Mn content the volume fraction of the phase decreases. That leads to a lower Vickers hardness. A reduction in the hardness may be observed in alloys with Mn wt. % from 6% to 13%. It means that the volume fraction of the ω phase affects the hardness measurements the most. When the Mn content reaches 18%, the Vicker's hardness increases again. This indicates that at high Mn content (13%), the solution hardening effect that is caused by atoms of Mn becomes the predominant. A similar dependency may be observed for Young's modulus [58].

2.3.7 Production methods of Ti-Mn alloys

Arc melting

Arc-melting is a traditional method for producing Ti-Mn alloys. This method is similar to the aforementioned arc-melting of Ti-Cu alloys. Kim *et al.* used this method to prepare Ti-5Mn/Ti-10Mn/Ti-15Mn/Ti-20Mn alloys [24]. Shibuya *et al.* also used this method to produce Ti-Mn alloys with V as the third element [59]. Singh and Schwarzer described a non-consumable arc melting process by which they produce Ti-0.4Mn and Ti-1.8Mn alloys. Non-conventional cold rolling techniques were used in this study - multi-step cross, unidirectional and multi-step reverse rolling [60].

Cold crucible levitation melting (CCLM)

A special CCLM furnace is used for this method. This induction melting furnace replaces a traditional crucible with Cu crucible cooled by water. High frequency currents are used to heat the metal. The CCLM process is done in high purity argon atmosphere. Such process was used by Santos *et al.* to fabricate Ti-Mn alloys (6, 8, 10, 12, 14, 16 and 18 wt.%) [58] and Ti-(5-6) Mn-(3-4)Mo alloys [61]. To produce ingots of Ti-Mn alloys, researchers used pure Ti chips and flakes of Mn (99.9% and higher). The ingots fabricated by CCLM underwent a homogenization treatment and later ice water quenching. After that, material was subjected to hot rolling and hot forging to get plates with required thickness. At last, the plates were solution treated in vacuum and once more ice water quenched.

Magnetic levitation melting (MLM)

Yu and coworkers applied MLM to produce $TiMn_{1.25-x}Cr_{0.25}V_x$ (x = 0, 0.2, 0.3, 0.4 and 0.5) alloy samples. In this method, in order to achieve homogeneity of the alloy, the ingot was turned over and remelted for four times. After that, the material crushed into powder in air [62].

Powder metallurgy

Metal injection moulding (MIM)

One of the possible techniques that can be used in laboratory to produce Ti-Mn alloys is metal injection moulding (MIM). This near-net shape fabrication method is based on a combination of powder metallurgy and plastic injection moulding. This method uses spherical shape Ti (gas-atomized) and fine Mn powders obtained by grinding and crushing flakes of Mn where the maximum particle size should not exceed 45 μm. These powders are premixed in a pot mill under argon atmosphere. Then the mixture of powders is mixed with an organic binder using a pressure-type kneading machine. After that, the compounds are injection moulded. The next step is to partially remove the binder with n-hexane and then perform thermal debinding. MIM provides an opportunity to control the grain diameters by changing the temperature during sintering. Hot-working and cold-working techniques are not necessary to refine the grain. This method was used by Cho *et al.* to produce new low-cost β- type Ti alloy with improved tensile strength. Ti-13Mn alloy was fabricated using this method. Additionally, in order to improve its mechanical properties, the material underwent cold-rolling process at 60% and 90% reduction ratios [63]. Similar method is described y by Santos *et al.*. Using MIM, researchers obtained six Ti-Mn alloys with different Mn content (8, 9, 12, 13, 15, 17 wt.%) [64].

Spark plasma sintering (SPS)

SPS method was used for preparation of Ti-5Mn alloy (foam). In this study, a mixture of Ti powder with Mn powder (5 wt. %) is wet-milled (in n-hexane media) using planetary ball milling system for 60 hours (15:1 ball/powder weight ratio, 300 rpm rotation rate). After that, NH_4HCO_3 (15 wt. %) and TiH_2 (2 wt. %) are added to the mixture. The mixture is poured into a graphite die for consolidation. Then, the die assembly is placed into a HPD-25/1 FCT SPS system [65].

2.3.8 Properties of Ti-Mn alloys

Ti-Mn alloys have higher density than pure Ti (4.50 g/cm^3). The density of the materials increases linearly with the increase of the Mn content. Ti-20Mn has density of 5.11 g/cm^3 [24]. The presence of pores, carbides and high oxygen content adversely influence the ductility of Ti-Mn alloys. As such, the improvement on this

mechanical property is required for the biomedical applications [64]. One of the solutions to overcome this issue is the addition of a third alloying element. Addition of 3-4 wt. % molybdenum into Ti-5Mn alloy improves the ductility of material by promoting mechanical twinning. Ti-Mn-Mo alloys (Ti-(5-6)Mn-(3-4)Mo) have better balance between ductility and strength [61]. Ti-Mn alloys have better UTS than Ti-64 ELI (1000 MPa). Ti-9Mn exhibits superior tensile properties (1048 MPa) to other similar Ti-Mn alloys [58]. With the addition of molybdenum as third element, it is possible to achieve even greater tensile properties. Ti-6Mn-3Mo has a UTS of 1220 MPa [61]. However, Young's modulus of Ti-Mn alloys are comparable or lower than of Ti-64 ELI (116-120 GPa) [58]. Among the Ti-Mn alloys, Ti-20Mn and Ti-5Mn possess the highest and the lowest Young's modulus [24]. Studies done by researchers revealed that all Ti-Mn alloys have higher values of Vickers hardness than pure Ti (165 HV) and Ti-64 ELI (325 HV) [58]. Ti-5Mn, Ti-9Mn, Ti-13Mn, Ti-18Mn exhibits Vickers hardness values of 345, 338, 312 and 336 HV respectively [24]. Hardness can be increased by the introduction of molybdenum as a third component. Ti-6Mn-4Mo has the highest hardness value of 373 HV [61].

Cold rolling of Ti-Mn alloys significantly increases various mechanical properties of the materials. Cho *et al.* observed that for Ti-13Mn alloy, factors such as the ultimate tensile strength, 0.2% proof stress, Vickers hardness and Young's modulus depend on the cold-rolling reduction ratio (0% to 90%). The cold workability of Ti-13Mn is good enough to withstand 90% cold-rolling process. Apart from this, the optical micrographs indicated that no cracks were formed during cold rolling [63]. As result of 90% cold-rolling process, the ultimate tensile strength increased from 888 MPa to 1852 MPa, 0.2% proof stress increased from 827 MPa to 1823 MPa, the Vickers hardness increased from 279HV to 461 HV and the Young's modulus from 96 GPa to 108 GPa [63].

Ti-Mn alloys show better corrosion resistance than pure Ti [65]. The addition of Mo leads to decrease in corrosion resistance but an addition of 3wt.% Mo permits to obtain a behaviour comparable to that of pure Ti [61].

CHAPTER 3

THE UNIVERSITY OF
WAIKATO
Te Whare Wānanga o Waikato

Experimental procedure

3.1 Materials

The raw materials used for this study include Ti, Cu and Mn powders. Some features of the raw materials and the details of the binary compositions designed are displayed on **Table 3.1** and **Table 3.2** respectively. In particular Ti-xCu (x = 0.5%, 2.5% and 5%) and Ti-yMn (y = 1%, 5% and 10%) were produced using the right ratio of powders as weighed on an analytical balance. The different binary Ti-Cu and Ti- Mn powder blends were mixed using a V blender (Figure 3.1) at a speed of 30 Hz for 30 minutes.

Table 3.1 Details of the raw materials used in this study.

Materials	Purity	Particle size	Supplier
Ti	99.4 %	200 mesh	Goodfellow Cambridge Lt, UK
Cu	99.7 %	230 mesh	Merck KGaA, Germany
Mn	99.0 %	-325 mesh	Sigma-Aldrich, NZ

Table 3.2 Details of the compositions and processing parameters used in this study.

Material		Sintering Temperature (^{o}C)	Forging Temperature (^{o}C)	
Composition	wt.%		α+β	β
Ti-Cu	0.5	1250	900	1150
	2.5		880	
	5		845	
Ti-Mn	1		900	
	5		800	
	10		690	

Figure 3.1 V-Blender used for mixing the raw powders.

3.2 Methods

3.2.1 Pressing

The mixed powders of the different compositions were shaped as cylindrical samples using a 40 mm diameter die and compaction was carried out with a hydraulic press. The compaction pressure of 795 MPa was adequate to produce pellets easy for handling for further processing.

3.2.2 Sintering

The samples were sintered by employing a conventional vacuum furnace. The temperature was increased at the rate of 10°C/min up to 1250°C and the holding time was 2 hours. Finally, the samples were cooled inside the vacuum furnace. The temperature profile used for sintering is shown in **Figure 3.2**.

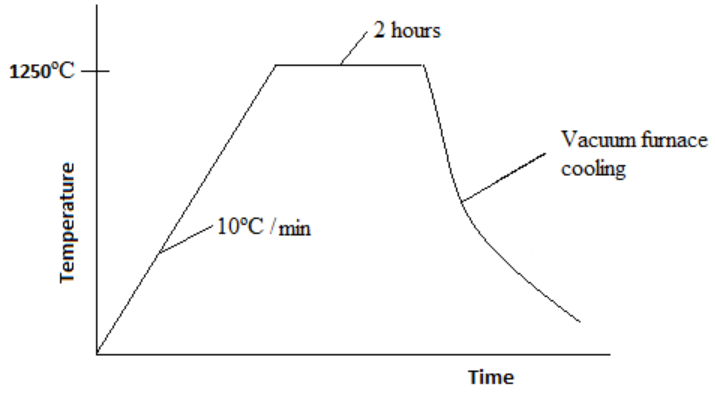

Figure 3.2 Temperature profile used for sintering.

3.2.3 Forging

In this study a total of twelve samples (two samples from each compositions) were forged by conventional α+β or β forging. Forging temperatures used for the former and the latter are tabulated in Table 2. It can be noticed that the β forging temperature was fixed at 1150°C to guarantee the each individual binary alloy is well above its β transus temperature. In the case of α+β forging, 30°C was added on top of the nominal β transus measured from the respective binary Ti-Cu and Ti-Mn phase diagrams to account for the loss during the process handling. α+β forging was planned to be performed right below the β transus temperature of each compositions.

3.2.4 Density *(ρ)*

Firstly the theoretical density of each composition was determined using the role of mixture as per Equation 1 as these values are needed for the calculation of the relative density of the green and sintered samples:

$$\rho_{mix} = \rho_{element\,(1)} \times \%_{element(1)} + \rho_{element\,(2)} \times \%_{element(2)} \quad (1)$$

Where ρ_{mix} is the mixture density (g/cm^3), $\rho_{element}$ is the density of the element (g/cm^3) and $\%_{element}$ is the percentage of the element in the alloy.

The dimensions of the green samples were measured using a digital calliper (2-decimal accuracy) and a high precision analytical scale (4-decimal digits). The values of the green density of each sample was determined by dividing the mass of the sample over its volume as per Equation 2. Average values were calculated from 3 measurements.

$$\rho_g = \frac{M}{V} \quad (2)$$

Where ρ_g is the green density (g/cm^3), M is the mass of the sample (g) and V is the volume of the compact (cm^3).

In the case of the consolidated materials, either sintered, α+β forged or β forged, their density wasmeasured using Archimedes principle by liquid displacement. In order to obtain the density of the samples, they were weighted in air as well as in water. Density values were calculated using Equation 3 and the final values are the average of three measurements.

$$\rho = \frac{W_{air}}{W_{air} - W_{water}} \times \rho_{water} \quad (3)$$

Where W_{air} is the weight of the sample in air (g), W_{water} is the weight of the sample in water (g) and ρ_w is the density of water at room temperature (0.977 g/cm^3).

Finally the densification parameter (Ψ) was determined by the difference between sintered density and green density divided by the difference between theoretical density and green density as per Equation 4:

$$\Psi = \frac{\rho_s - \rho_g}{\rho_t - \rho_g} \times 100 \quad (4)$$

Where ρ_s is the sintered density (g/cm^3), ρ_g is the green density (g/cm^3) and ρ_t is the theoretical density (g/cm^3).

3.2.5 Tensile properties

Dog-bone tensile testing samples with rectangular cross section of 2x2 mm^2 and a gauge length of 20 mm (shown in Figure 3.3) were made using EDM wire cutter. Tensile tests were done on an Instron 33R4204 machine with a cross head speed of 0.1 mm/min.

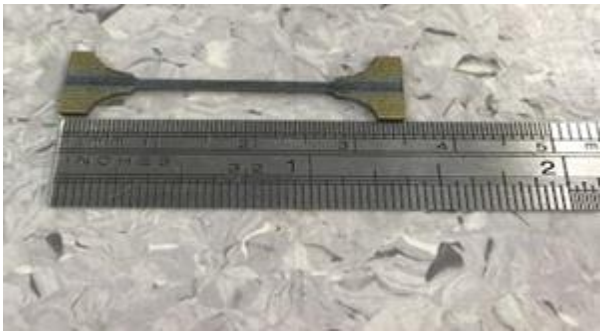

Figure 3.3 Geometry of the tensile testing sample.

3.2.6 Optical Microscopy (OM)

To determine the distribution and shape of the residual porosity, optical microscopic images were captured with a Nikon digital camera attached to an Olymbus BX60F5 microscope. In order to obtain optical images all samples were cut, ground and polished using an EDM wire cutter, Struess ROTOPO1201 grinding machine and Struess TEGRAMIN-25 automatic polishing machine respectively. Images were also captured for all samples after etching with Kroll's solution, consisting of 2 ml HF, 6 ml HNO_3 and 92 ml distilled water.

3.2.7 X-ray Diffraction (XRD)

XRD is a common technique used for the determination of crystallographic structure and it was used to identify and confirm the phases constituting each binary Ti-Cu and Ti-Mn alloy after the different processing routes. XRD analysis was carried out using a Philips X'Pert diffractometer (Cu Kα radiation - 1.54nm) within a scanning range of 5^o to 100^o at 45 kV and 40 mA with scan step size of 0.013^o.

3.2.8 Scanning Electron Microscopy (SEM)

The investigation of the microstructure of samples was done using Hitachi S4700 scanning electron microscope (SEM) equipped an energy dispersive X-ray spectrometer (EDS) used to take elemental chemical analysis measurements. Prior to the analysis at the SEM, the samples were coated by a thin layer of carbon.

3.2.9 Hardness

Hardness measurements were performed on the cross section of the materials using a Rockwell A tester. Three measurements were done for each samples in order to obtain repeatable results. Finally, the measurements were transformed to Vickers hardness as this hardness scale is more relevant for Ti alloys.

CHAPTER 4

THE UNIVERSITY OF
WAIKATO
Te Whare Wānanga o Waikato

Results and discussion

The different Ti-Cu and Ti-Mn alloys were processed through three conditions: sintering at 1250°C, β forging at 1150°C and α+β forging at different temperatures as indicated in Table 2. Therefore, the results are shown and discussed in three sections: as-sintered, β forged and α+β forged. In these three sections, the results of the characterisation of the six different Ti-Cu (i.e. Ti-0.5Cu, Ti-2.5Cu and Ti-5Cu) and Ti-Mn (i.e. Ti-1Mn, Ti-5Mn and Ti-10Mn) alloys is considered.

The discussion starts with the results of the relative densities of each composition. Secondly, the microstructure analysis performed at the SEM and OM to obtain the porosity distribution, size, and shape is presented. The microstructural analysis also considers the discussion of the phases of the alloys. In addition, the XRD patterns are presented to confirm the phases composing the alloys.

Finally, the results of the characterisation of the mechanical properties including Yield Strength (YS), Ultimate Tensile Strength (UTS), elongation and hardness are presented.

4.1 Properties of as-sintered binary Ti-Cu and Ti-Mn alloys

Sintering is a critical step in powder metallurgy and a temperature of 1250°C was chosen for sintering all samples in this study. This temperature was selected with the aim of achieving homogenous compositions of the samples, but it is paramount to quantify the effect of sintering on the density and geometry of the samples if the process has to be applicable in industry. The variation of the green and sintered density as well as that of the densification of the samples of the binary Ti-Cu and Ti-Mn alloys is presented in Figure 4.1a) and Figure 4.1b), respectively. As can be seen, the relative green density decreases when increasing alloying element content in the material regardless of the nature of the alloying elements. For Ti-Cu alloy, the relative green densities of the pressed powder compacts diminishes from 83.7% to 79.5% with the increment of the amount of Cu. Similarly,

in the case of the Ti-Mn alloys, the green density decreases from 85.0% to 79.2% as the amount of Mn increases.

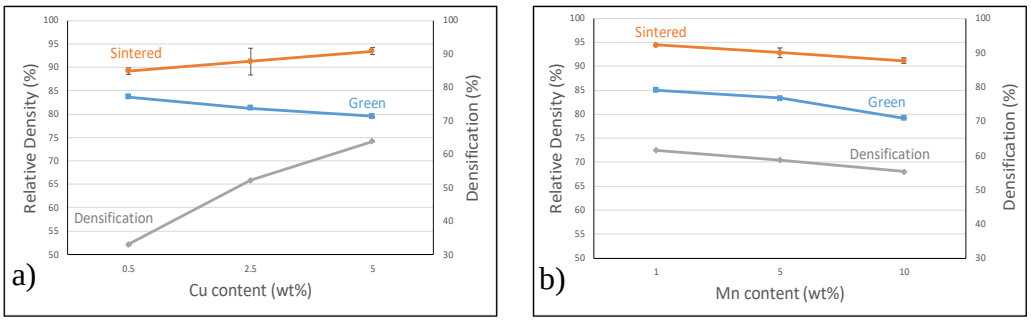

Figure 4.1 Relative densities and densification of the sintered Ti-Cu (a), and Ti-Mn (b) alloys.

The decreases of the relative green densities with the increment of the content of the alloying elements depends on the features of the raw powder, which were therefore analysed via SEM. From Figure 4.2, Ti, Cu and Mn powders are irregular with particle size of 75µm, dendritic with particle size of 45 µm and irregular with particle size of 63 µm respectively. The difference in morphology, particle size and deformability of the three powders determined the values of green density achieved.

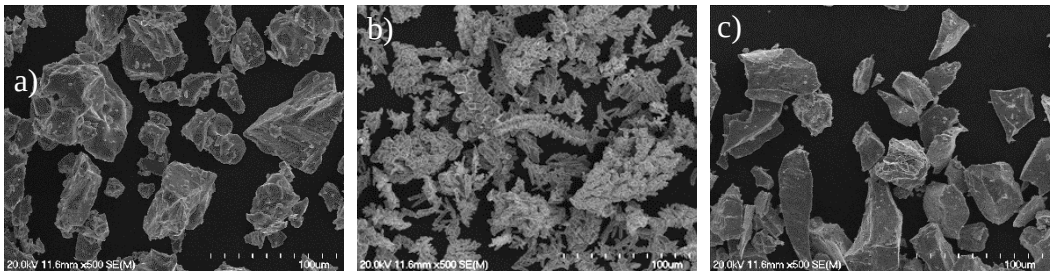

Figure 4.2 Morphology of the raw powders: a) Ti, b) Cu and c) Mn.

Sintering of the samples using a vacuum furnace resulted in an increment of the density with respect to the green samples. On the one hand, sintered Ti-Cu samples had relative densities between 88.2% and 93.4% and the density increases with the Cu content. On the other hand, Ti-Mn samples had slightly higher sintered relative densities, reaching a maximum value of 94.4%, but the density decreases with the amount of Mn. Sintering does not only induce the reduction of the porosity (i.e. increment of the density) but also provokes the shrinkage of the samples and this can be quantified via the densification parameter. From Figure 4.1b), the

densification rises rapidly from 33.0% to 63.9% as the Cu content increases, but gradually drops from 61.5% to 55.3% for the Ti-Mn alloys.

The results of the microstructural characterisation for the Ti-Cu and the Ti-Mn alloys are shown in **Figure 4.3** and Figure 4.4, respectively. From the OM micrographs of **Figure 4.3**a), c) and e), the Ti-0.5Cu, Ti-2.5Cu and Ti-5Cu have mainly close spherical pores, with size in the range between 15 and 200μm, and a small number of irregular pores. It is worth mentioning that some few large pores (~200μm) are present near the surfaces of the samples, whereas small pores are present in the middle of the materials as per the micrographs presented. It can also be seen that all the Ti-Cu alloys have lamellar microstructure (**Figure 4.3** b), d) and f). Microstructure analysis shows that the thickness of β phase in Ti-0.5Cu and Ti-2.5Cu is low (about 2-8 μm), while in the Ti-5Cu is relatively thicker (about 10-18 μm) as a consequence of the increased addition of the β stabilizer.

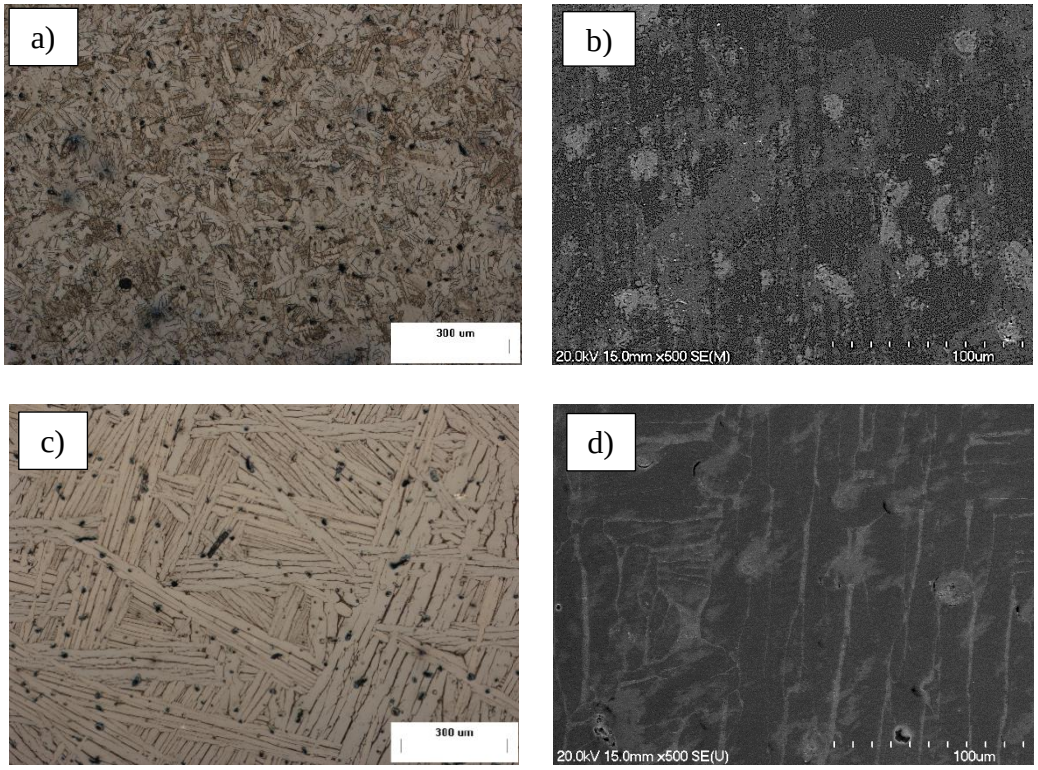

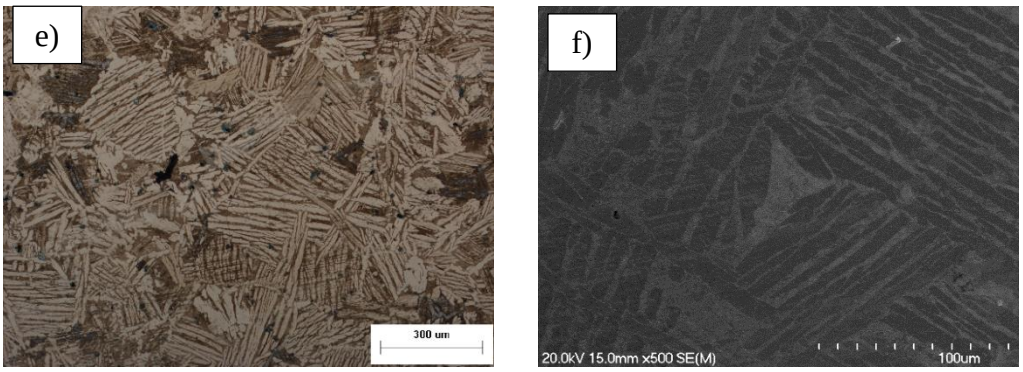

Figure 4.3 Optical micrographs and SEM images of the sintered Ti-Cu alloys: a) and b) Ti-0.5Cu, c) and d) Ti-2.5Cu, and e) and f) Ti-5Cu.

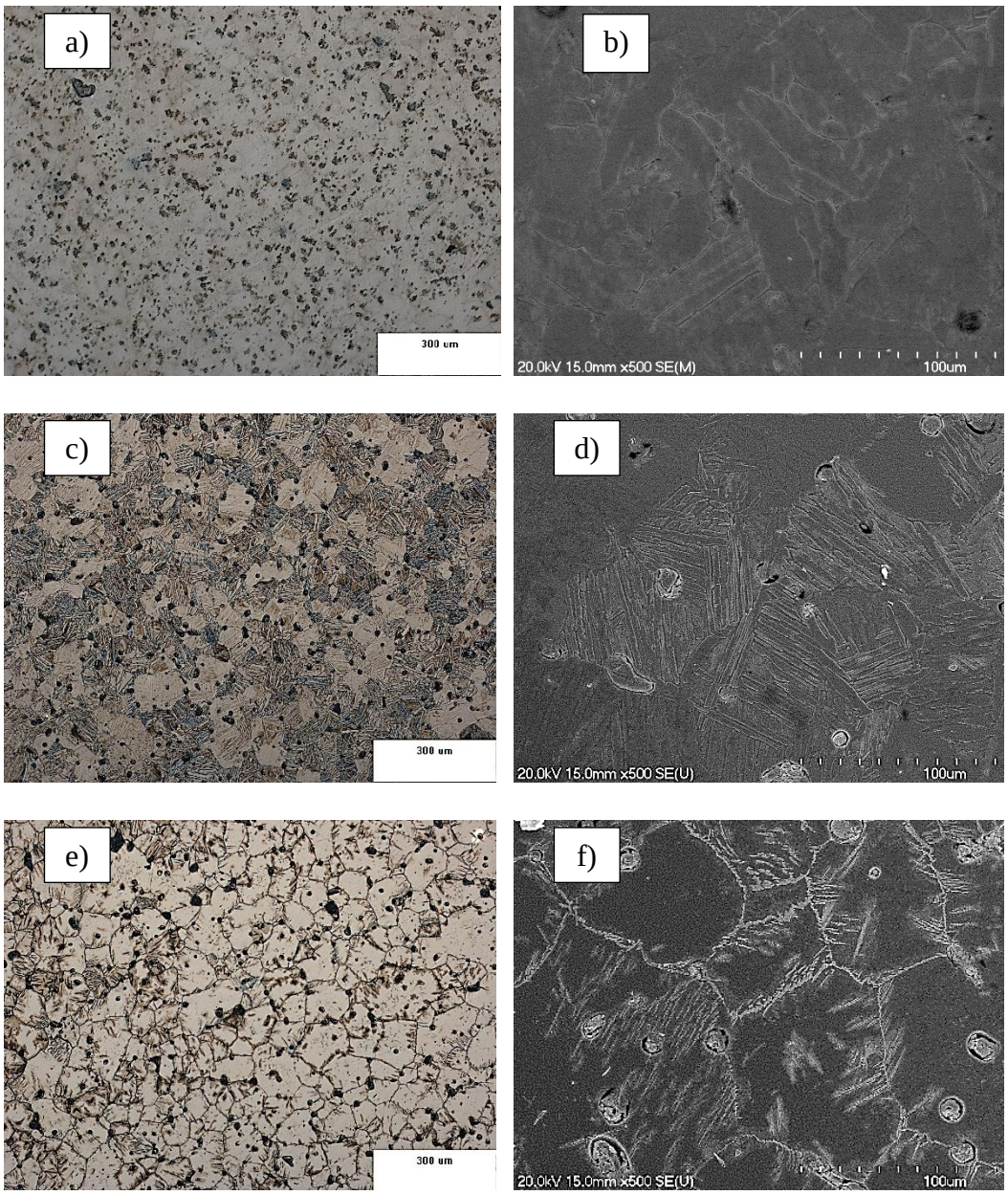

Figure 4.4 Optical micrographs and SEM images of the sintered Ti-Mn alloys: a) and b) Ti-1Mn, c) and d) Ti-5Mn, and e) and f) Ti-10Mn.

From Figure 4.4, the sintered Ti-1Mn and Ti-5Mn have a pore size in the range between 15 and 200 μm, a lamellar microstructure and primarily closed spherical pores. In the case of the Ti-10Mn (Figure 4.4 e and f) the sintered alloy has also close porosity, but the microstructure is mainly composed of equiaxed β phase grains (15-170 μm) rather than a lamellar structure. In all the sintered Ti-Cu and Ti-Mn alloys the great majority of the pores are close porosity indicating that the third stage of sintering was achieved during the sintering of the alloys at 1250oC for two hours. No undissolved powder particles were found during the microstructural analysis and the microstructures are homogeneous.

The complete dissolution and homogenisation of the alloying elements was further proved via EDS analysis and the results are shown Table 4.1 and Table 4.2 for the sintered Ti-Cu and Ti-Mn alloys, respectively.

Table 4.1 Results of the EDS chemical analysis of the sintered Ti-Cu alloys.

Alloy	**Ti-0.5Cu**	**Ti-2.5Cu**	**Ti-5Cu**
Ti content (wt.%)	99.65 ± 0.5	96.95 ± 0.5	95.27 ± 0.5
Cu content (wt.%)	0.35 ± 0.5	3.05 ± 0.5	4.73 ± 0.5

Table 4.2 Results of the EDS chemical analysis of the sintered Ti-Mn alloys.

Alloy	**Ti-1Mn**	**Ti-5Mn**	**Ti-10Mn**
Ti content (wt.%)	99.06 ± 0.5	94.99 ± 0.5	90.53 ± 0.5
Mn content (wt.%)	0.94 ± 0.5	5.01 ± 0.5	9.47 ± 0.5

As shown in Figure 4.5, in the XRD patterns of the Ti-0.5Cu and Ti-2.5Cu alloys sintered at 1250^{o}C, only the α phase was detected whereas the Ti-5Cu alloy has also peaks corresponding to the β phase and the Ti_2Cu intermetallic. It can be noticed that the amount of β phase retained in the Ti-0.5Cu and Ti-2.5Cu after the cooling from the sintering temperature is relatively low and thus the β phase was not detected during XRD due to the resolution of the equipment.

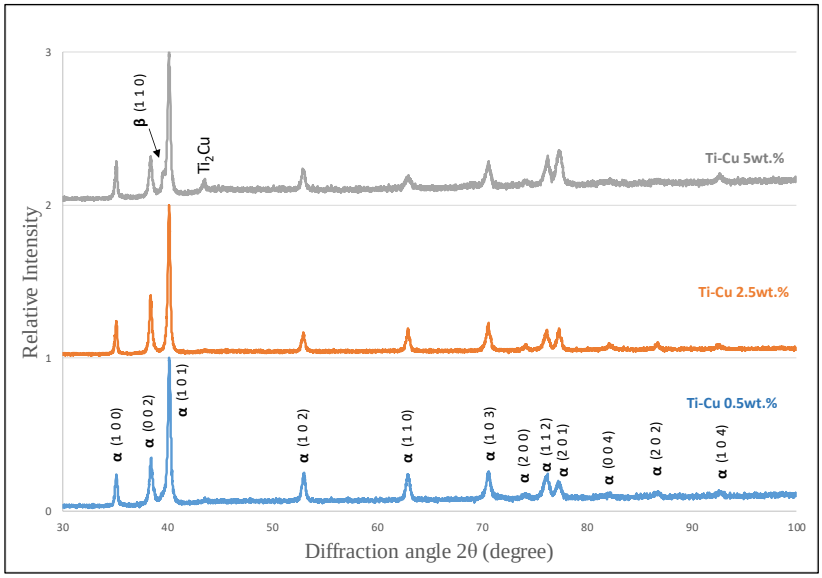

Figure 4.5 XRD patterns of the sintered Ti-Cu alloy.

From Figure 4.6, the XRD pattern of Ti-1Mn alloy sintered at 1250°C has only α phase. In the case of the Ti-5Mn alloy, the main peak of the β phase was also detected whereas for the Ti-10Mn alloy only peaks of the β phase are present.

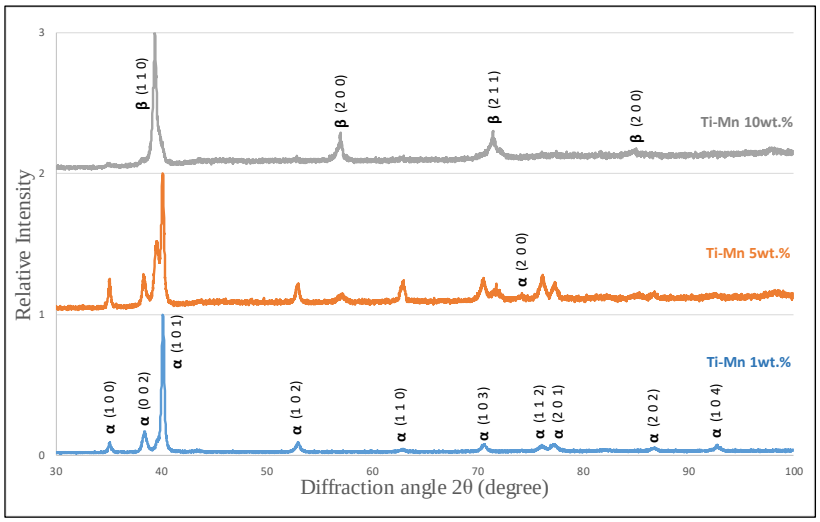

Figure 4.6 XRD patterns of the sintered Ti-Mn alloy.

Figure 4.7 shows representative stress-strain curves of the sintered Ti-Cu and Ti-alloys, whereas it can be seen that as the Cu and Mn content is increased the strength increases but the elongation decreases. In addition, the Young's modulus has been calculated to be 98 GPa, 92 GPa and 103 GPa for Ti-0.5Cu, Ti-2.5Cu and Ti-5Cu respectively; whilst for the Ti-Mn alloys the Young's modulus values are 92 GPa, 95 GPa and 100 GPa for Ti-1Mn, Ti-5Mn and Ti-10Mn respectively. In comparison to pure Ti, it is obvious that the Ti-Cu alloys always have higher strength and

elongation, whereas the Ti-Mn alloys have higher strength but the elongation is only significantly improved in the case of the Ti-1Mn alloy.

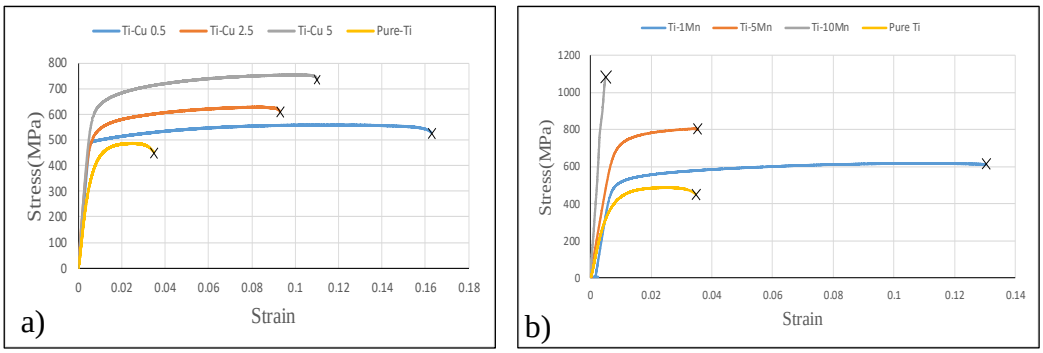

Figure 4.7 Stress-strain curves of the sintered Ti-Cu (a) and Ti-Mn (b) alloys.

Figure 4.8 a) shows that the UTS and YS increase along with the content of Cu. The UTS increases from 554 MPa to 753 MPa and the YS increases from 467 MPa to 627 MPa. The increment found is consistent with the current literature [59]. However, the elongation decreases as the Cu content increases, as the elongation drops from 15% to 9% due to the Ti_2Cu phase which is the intermetallic phase that has been found from the XRD pattern for Ti-Cu in Figure 4.5. It also can be seen that the Ti_2Cu phase is found when the Cu content is increased, but few previous studies have detected the same behaviour for Ti-Cu alloy [42].

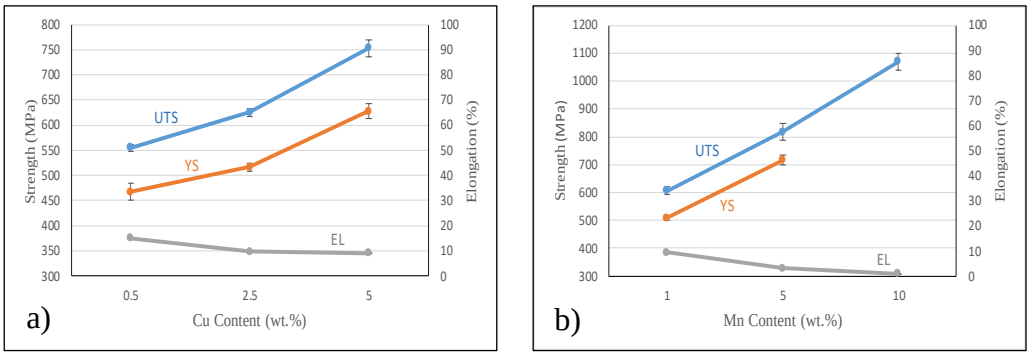

Figure 4.8 Variation of the tensile properties (UTS, YS and EL) with the amount of alloying element for sintered Ti-Cu (a) and Ti-Mn (b) alloys.

Similarly, Figure 4.8 b) shows that there is an increase in UTS and YS with the Mn content, as the UTS increases from 606 MPa to 1070 MPa and the YS increases from 508 MPa to 716 MPa. However, no YS could be determined, as the Ti-10Mn is a purely elastic material and failed with no plastic deformation. Finally, the elongation also has a sharp decrease from 9.3% to 0.87% and this is thought to be due to the formation of the ω phase which can only by detected via TEM analysis.

Studies available in the literature suggest that this phase should be present as the brittle ω phase is formed in Ti-6Mn and Ti-9Mn alloys [24].

The results of the hardness measurements show that there is a linear relationship between the hardness of the sintered samples and the Cu and Mn content (Figure 4.9). Precisely, the hardness rises from 174.0 to 227.0 and from 180.0 to 336.7 as the Cu and Mn content rises respectively.

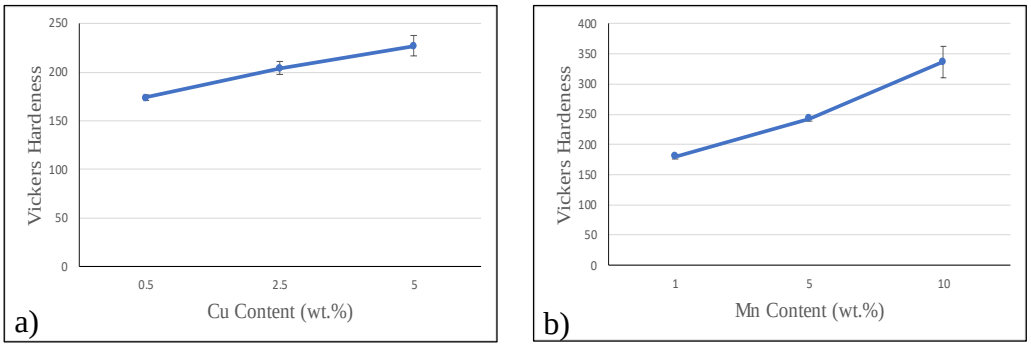

Figure 4.9 Vickers hardness of the sintered Ti-Cu (a) and Ti-Mn (b) alloys.

4.2 Properties of β forged binary Ti-Cu and Ti-Mn alloys

The variation of the relative density after the β forging process in shown in Figure 4.10 where it can be seen that the relative density increased from 98.8% to 99.6%, followed by a decrease of 0.9% for the Ti-Cu alloys. For the Ti-Mn alloys, the relative density dropped slightly from 99.2% to 98.1%, then increased again as the Ti-Mn alloy increased from 5wt.% to 10wt.% to 99.0%. From Figure 4.10a), forging after sintering induced an increase in relative densities of at least 5.29% at Ti-5Cu and a maximum of 9.88% at Ti-0.5Cu, and an increase between 3.77% and 7.79% of the relative density of the Ti-Mn alloys as the Mn content increases from 1wt.% to 10wt.%. The increase in relative densities is attributed to the disappearance of most of the pores achieved via forging.

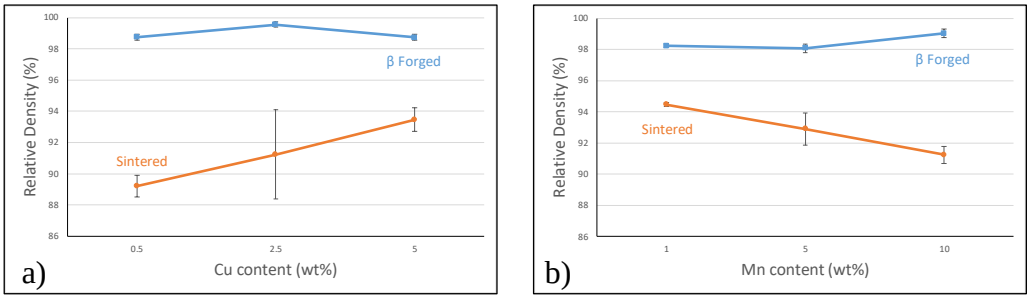

Figure 4.10 Relative densities and densification of the β forged Ti-Cu (a), and Ti-Mn (b) alloys.

The results of the microstructural characterisation of the β forged Ti-Cu and Ti-Mn alloys are presented in Figure 4.11. The OM results show that the Ti-0.5Cu, Ti-2.5Cu and Ti-5Cu have a pore size in the range between 2.5 and 85 µm, the porosity has mainly needle-like shape but there are a minority of spherical pores left by the forging process. From the microstructural analysis it is found that the Ti-0.5Cu, Ti-2.5Cu and Ti-5Cu alloys have a martensitic microstructure (Figure 4.11 b, d and f). The formation of the α' martensitic phase is thought to be the consequence of the fast cooling that the alloys experience during the forging process as cooling happens from a temperature in the β field. It can be noticed that the number and features of the needle-like grains increases with the amount of Cu content of the alloys.

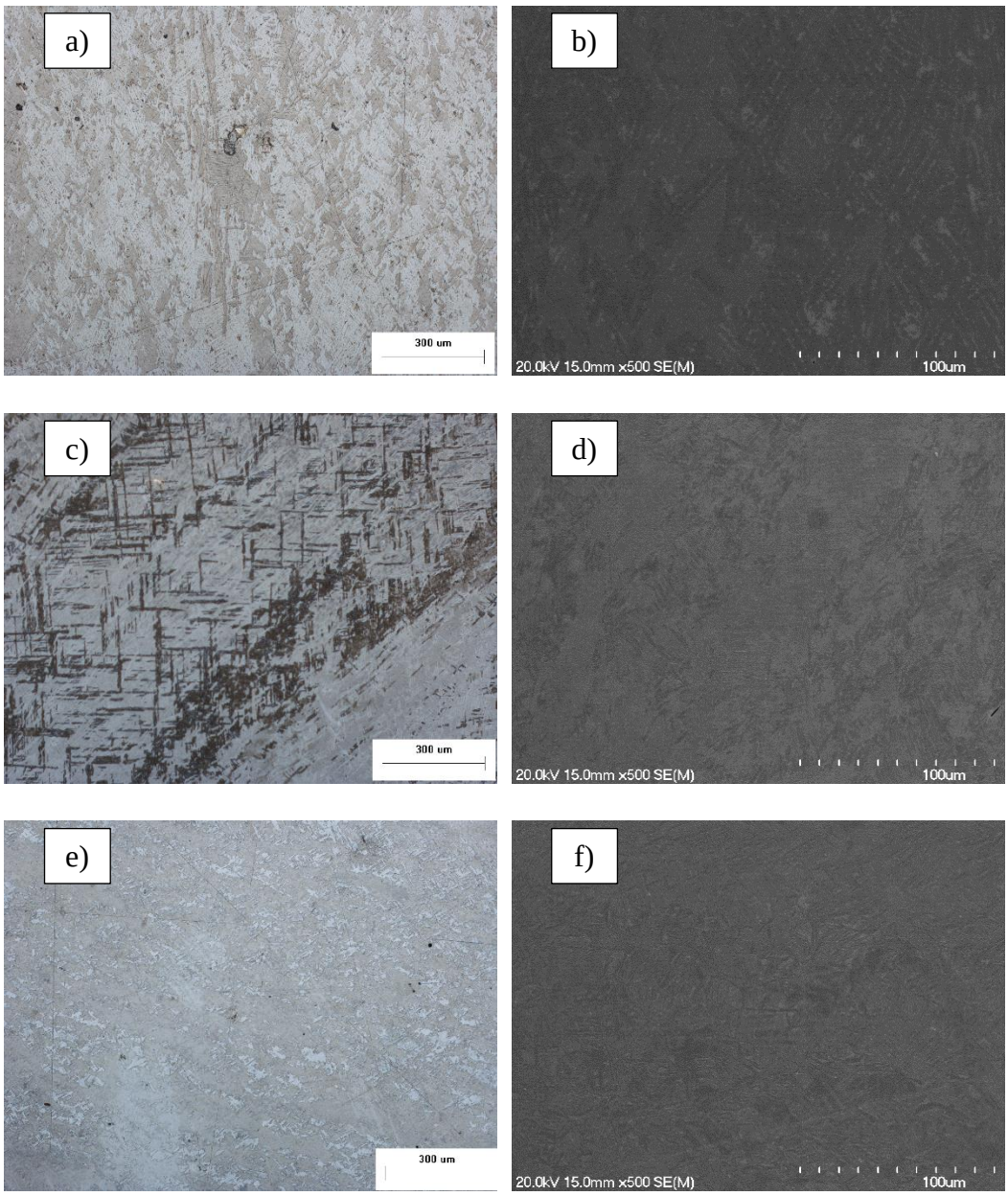

Figure 4.11 Optical micrographs and SEM images of β forged Ti-Cu alloys: a) and b) Ti-0.5Cu, c) and d) Ti-2.5Cu, and e) and f) Ti-5Cu.

From Figure 4.12 a), c) and e), the Ti-Mn have pores of size in the range between 2.5 and 130 µm, and once again the residual porosity has a needle-like appearance as consequence of the forging process, but a small number of spherical pores are present. Similar to Ti-Cu alloys, martensite is formed in the lower alloyed Ti-Mn alloys (i.e. Ti-1Mn and Ti-5Mn), whereas the Ti-10Mn have a microstructure composed of elongated β grains (Figure 4.12 b, d and f). Thus, comparing these results with the results of as sintered, the type of the microstructure has been significantly changed and this would affect the mechanical behaviour of the materials.

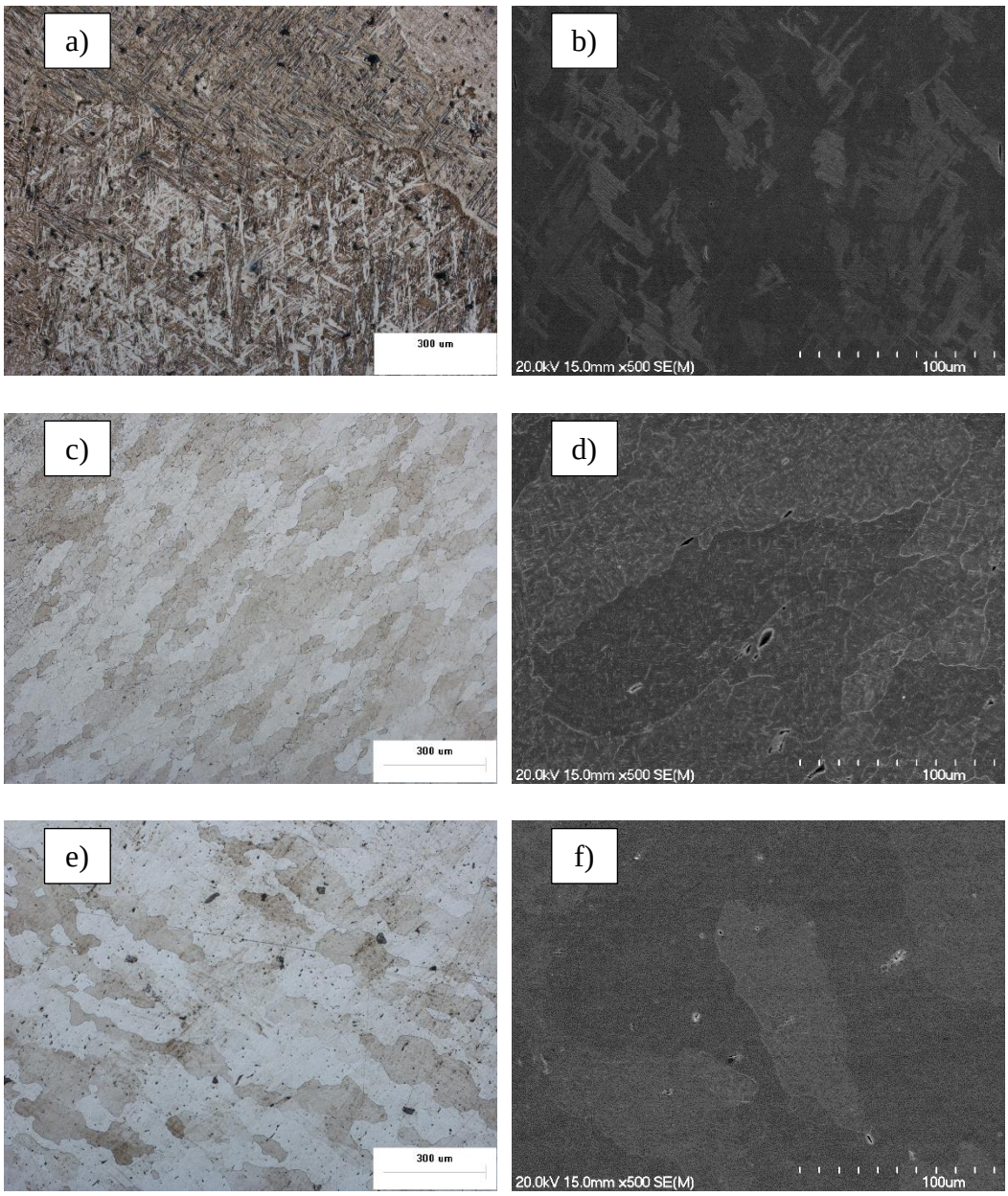

Figure 4.12 Optical micrographs and SEM images of β forged Ti-Mn alloys: a) and b) Ti-1Mn, c) and d) Ti-5Mn and e) and f) Ti-10Mn.

The XRD patterns of the β forged Ti-0.5Cu and Ti-2.5Cu alloys have only α phase (Figure 4.13) whereas Ti-5Cu has α and β phase and a peak of the Ti_2Cu phase. No singificant changes are found with respect to the sintered samples apart from that the intensity of the Ti_2Cu phase is lower due to its dissolution during the heating of the material prior to its forging. It is worth mentioning that the α' martensitic phase has equivalent lattice to that of the α phase, and therefore their XRD peaks have the same 2θ positions in the XRD patterns.

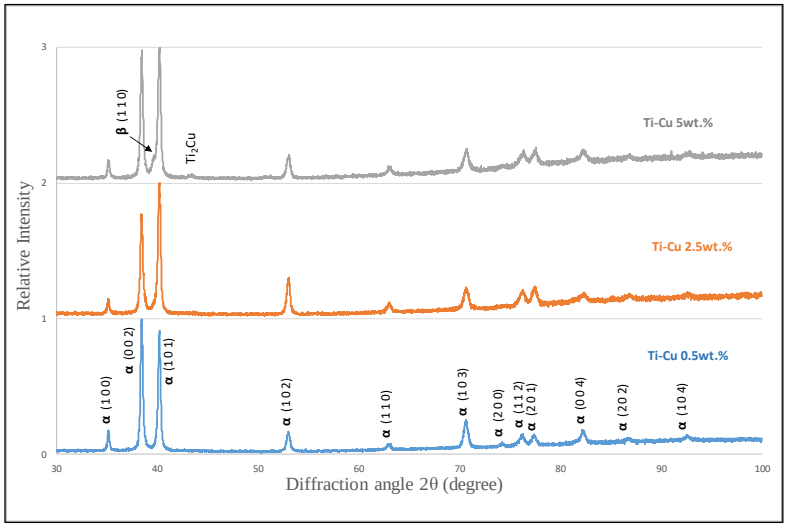

Figure 4.13 XRD patterns of the β forged Ti-Cu alloy.

The XRD patterns of the β forged Ti-1Mn alloy (Figure 4.14) has α phase, while Ti-5Mn and Ti-10Mn alloys have α and β phase mainly α and mainly β respectively. Lastly, an extra peak was detected in the Ti-5Mn at 98°, which is believed to be β phase [66].

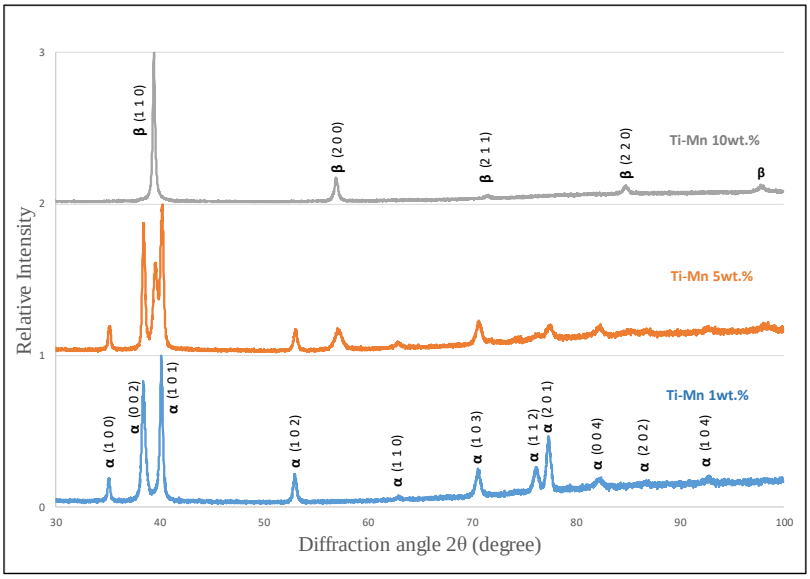

Figure 4.14 XRD patterns of the β forged Ti-Mn alloy.

It is also worth noting that from the comparison of the XRD patterns of **Figure 4.5** Figure 4.5, Figure 4.13 and Figure 4.13 it is found that α (0 0 2) for both Ti-Cu and Ti-Mn alloys has incresed significantly from the sintered to the β forged alloys, and this is due to the texture imposed on the materials by the uniaxial force applied during the forging proccess.

Representative stress vs strain graphs of the β forged Ti-Cu alloys are shown in Figure 4.15 a) where all the forged alloys have improved strength and elongation with respect to pure Ti. In the case of the Ti-2.5Cu alloy, two curves are presented as a significant different behaviour was found when testing material cut from the middle or from near the surface of the forged sample. Fully dense material was obtained in the middle of the sample (Figure 4.16 a) and consequently the maximum detectable elongation of 23% without failure was achieved with this material. Nevertheless, the material cut from near the surface has a much higher amount of residual porosity left (Figure 4.16 b) and it fractured at 8.4% of elongation.

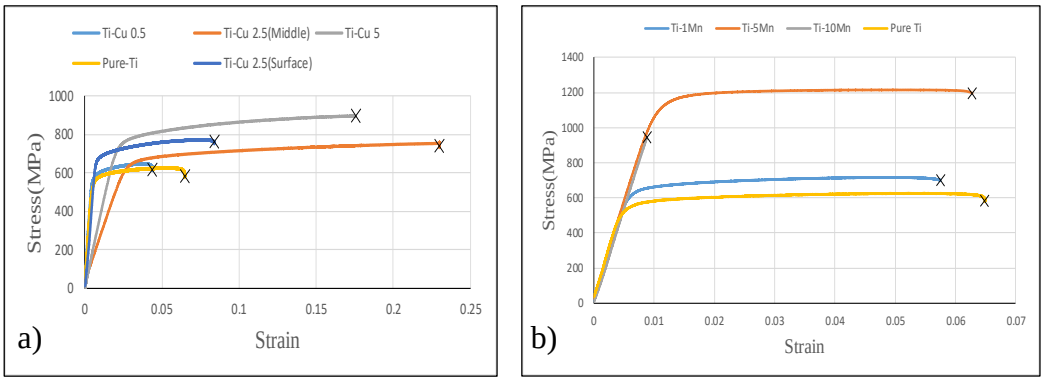

Figure 4.15 Stress-strain curves of the β forged d Ti-Cu (a) and Ti-Mn (b) alloys.

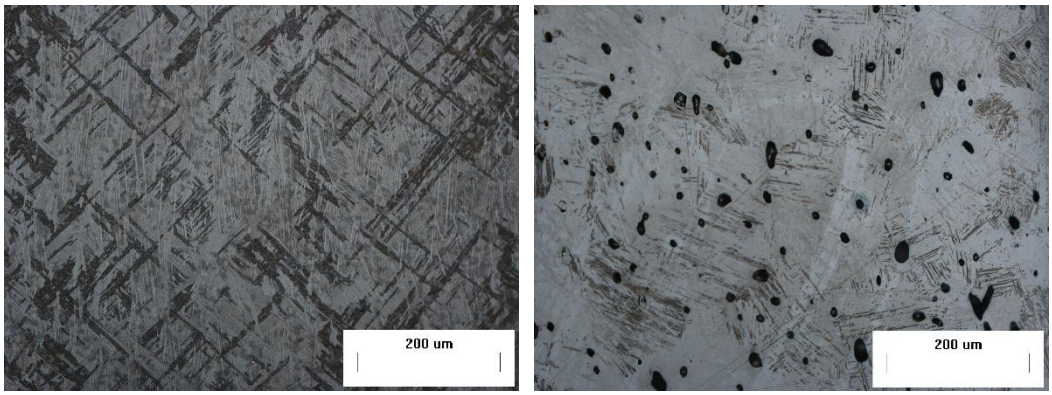

Figure 4.16 Optical micrographs of β forged Ti-2.5Cu alloy: middle of the forged sample, and b) near the surface of the forged sample.

Figure 4.17 a) illustrates the relationship between the Cu content and the UTS, YS and elongation of the material. As can been, when the amount of Cu increases the UTS and YS increase as well. The UTS slightly increases from 649 MPa to 728 MPa when the Cu content is increased from 0.5wt.% to 2.5wt.%, followed by a rapid increase to reach 905 MPa at 5wt.%. In addition, Figure 4.17 a) also shows a

slight increase in YS from 602 MPa to 642 MPa and then to 757 MPa. Regarding the elongation, there is an initial increase from 3% to 18% followed by a decrease to 13.3%.

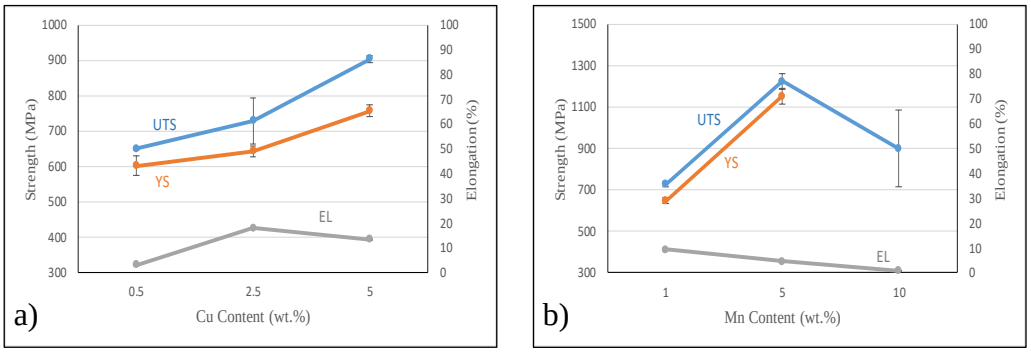

Figure 4.17 Variation of the tensile properties (UTS, YS and EL) with the amount of alloying element for β forged Ti-Cu (a) and Ti-Mn (b) alloys.

The inverted V-shape trend for the elongation could be explained by the fact that when the Cu content increases, the stability of the β region increases as well, which leads to decrease in the β transus temperature. This means that there is more time for Ti-2.5Cu alloy to deform, which was an advantage for the material to close most of the pores, especially in the middle. Another potential explanation can be found by considering the fracture toughness of the material $Kc = Y\sigma_c \sqrt{\pi a_c}$ (where Y= geometry, σ_c = applied stress, a_c = crack length). The length of the α' martensitic grains of the Ti-0.5cu is lower than that of the grains of the Ti-2.5Cu alloy (Figure 4.11 a and c). Applying that change of length on the fracture toughness formula will affect the value of Kc, which will affect the elongation.

Figure 4.17 b) displays a rise in UTS from 728 MPa to 1224 MPa as the Mn content increases from 1wt. % to 5wt.%. However, this time the UTS falls noticeably to reach 899 MPa. As discussed previously, the embrittlement of the Ti-10Mn alloys is due to the presence of the brittle ω phase. Regarding the YS, it increases sharply from 648 MPa to 1145 MPa, but no yield point could be measured for the Ti-10Mn alloy. Finally, the elongation falls sharply from 9.3% to 0.8% as the Mn content increases.

In comparison to the sintered alloys, the results of the characterisation of the β forged materials indicate that higher UTS and YS values are achieved irrespective of the Cu and Mn contents. Conversely, the elongation of the β forged alloys is

generally lower for the Ti-Cu alloys, but fairly similar in the case of the Ti-Mn alloys when compared to the values of the respective sintered materials.

The variation of the hardness of the β forged Ti-Cu and Ti-Mn alloys is plotted in Figure 4.18 and it can be seen that as Cu content increases, the hardness increases as well from 235.3 to 302.7. On the other hand, the hardness increases from 218.7 to 415.7 as the Mn content increases from 1wt.% to 5wt.%, followed by a gradual decrease until it reaches 397.7 (Figure 4.18 b).

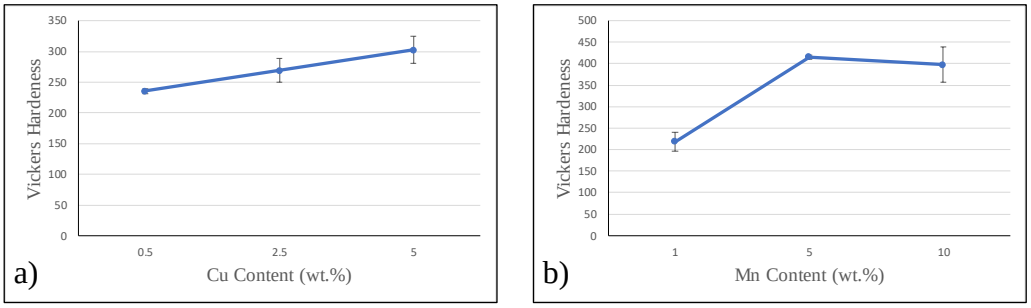

Figure 4.18 Vickers hardness of the β forged Ti-Cu (a) and Ti-Mn (b) alloys.

4.3 Properties of α+β forged binary Ti-Cu and Ti-Mn alloys.

The results of the relative density of the Ti-Cu and Ti-Mn alloys subjected to α+β forging are presented in Figure 4.19 a) and b respectively. It can be seen that the relative density after α+β forging rises slightly from 98.78% to 99.03%, then it drops down to reach 98.37% as the Cu content increases from 0.5wt.% to 5wt.%. Likewise, Figure 4.19 b shows firstly a slow increase from 99.15% to 99.25%, followed by a gradual decrease to 98.71%.

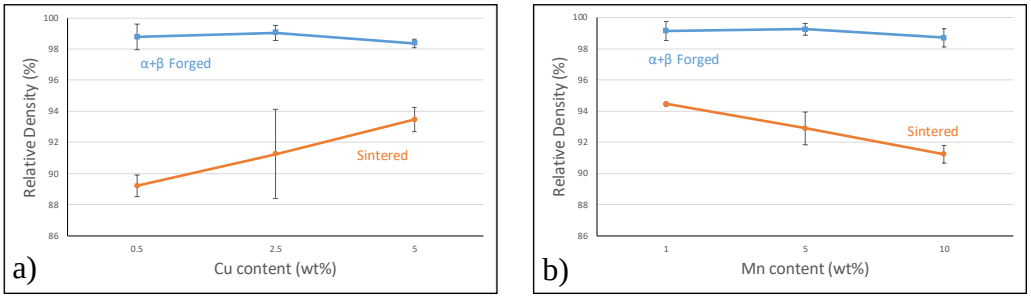

Figure 4.19 Relative densities and densification of the α+β forged Ti-Cu (a), and Ti-Mn (b) alloys.

Therefore, α+β forged relative density values increase by a fair amount in comparison to the values of the sintered materials. In view of the results obtained, the relative density rises from 89.21% (sintered) to 98.78% (α+β forged) for the Ti-0.5Cu alloy and the difference in relative density between the sintered and the α+β forged alloys gradually decreases until it reaches a difference of 4.91% as the Cu content increases. Moreover, as the Mn content increases from 1wt.% to 10wt.%, the difference in relative density increases from 4.69% to 7.48% when comparing sintered and α+β forged alloys.

In the case of the α+β forging, the optical micrographs shown in Figure 4.20 a), c) and e), indicate that Ti-0.5Cu, Ti-2.5Cu and Ti-5Cu alloys have needle-like pore (size in the range between 2.5 and 90 µm) and small numbers of spherical pores are present such as after β forging. From Figure 4.20 b), d) and f) the Ti-0.5Cu, Ti-2.5Cu and Ti-5Cu alloys have a martensitic microstructure. As for β forging, the α' martensitic phase is formed due to the fast cooling that the alloys experience during the forging process.

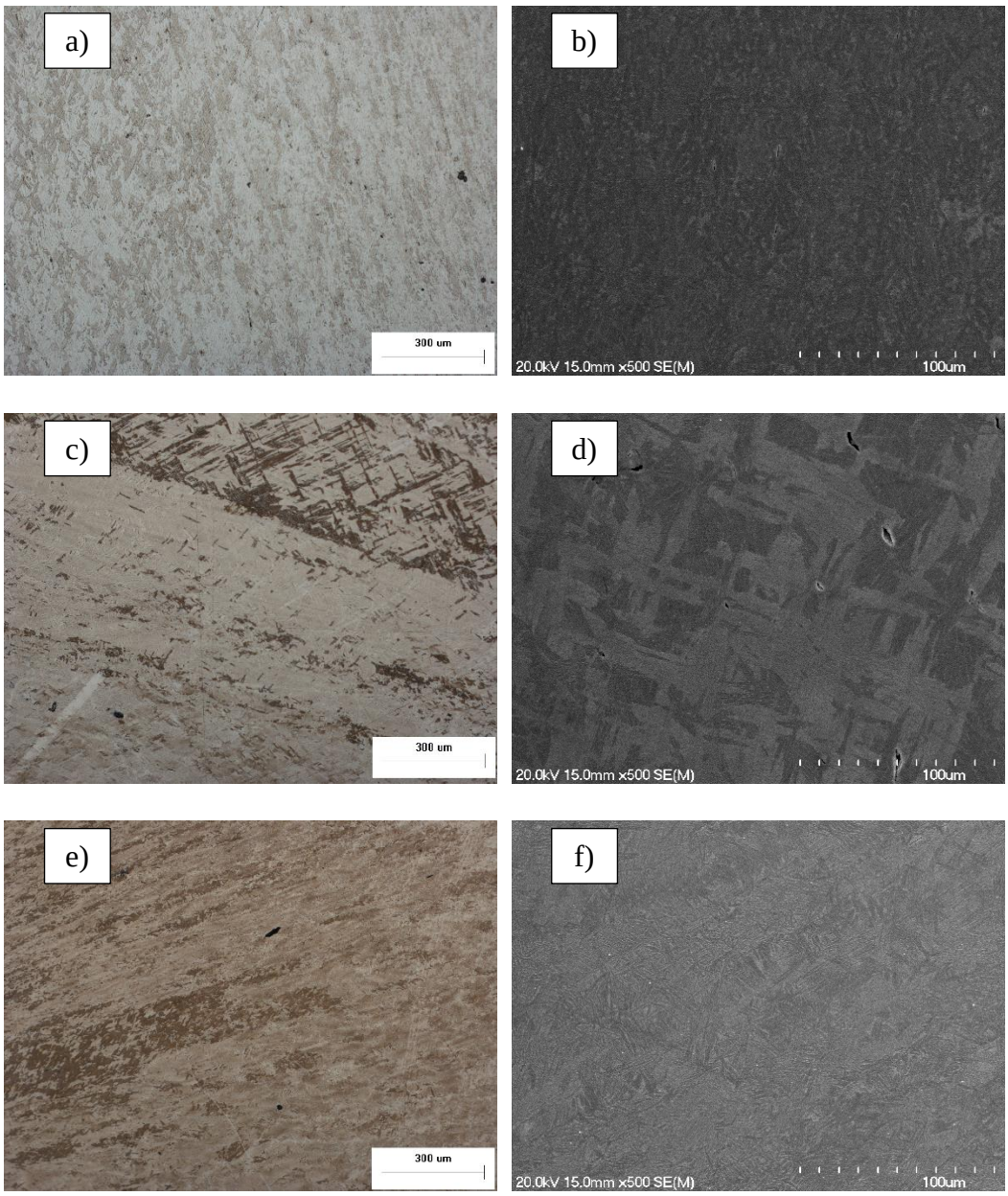

Figure 4.20 Optical micrographs and SEM images of α+β forged Ti-Cu alloys: a) and b) Ti-0.5Cu, c) and d) Ti-2.5Cu, and e) and f) Ti-5Cu.

In the case of the α+β forged Ti-Mn alloys (Figure 4.21 a, c and e), Ti-1Mn, Ti-5Mn and Ti-10Mn have a pore size in the range between 2.5 and 100 µm, 2.5 and 130 µm and 2.5 and 130 µm respectively. Once again the majority of the pores are needle-like with a small percentage of spherical pores. From the SEM analysis (Figure 4.21 b, d and f), martensite is present in the microstructure of the Ti-1Mn and Ti-5Mn alloys whilst elongated β grains are the main constituent of the α+β forged Ti-10Mn alloy.

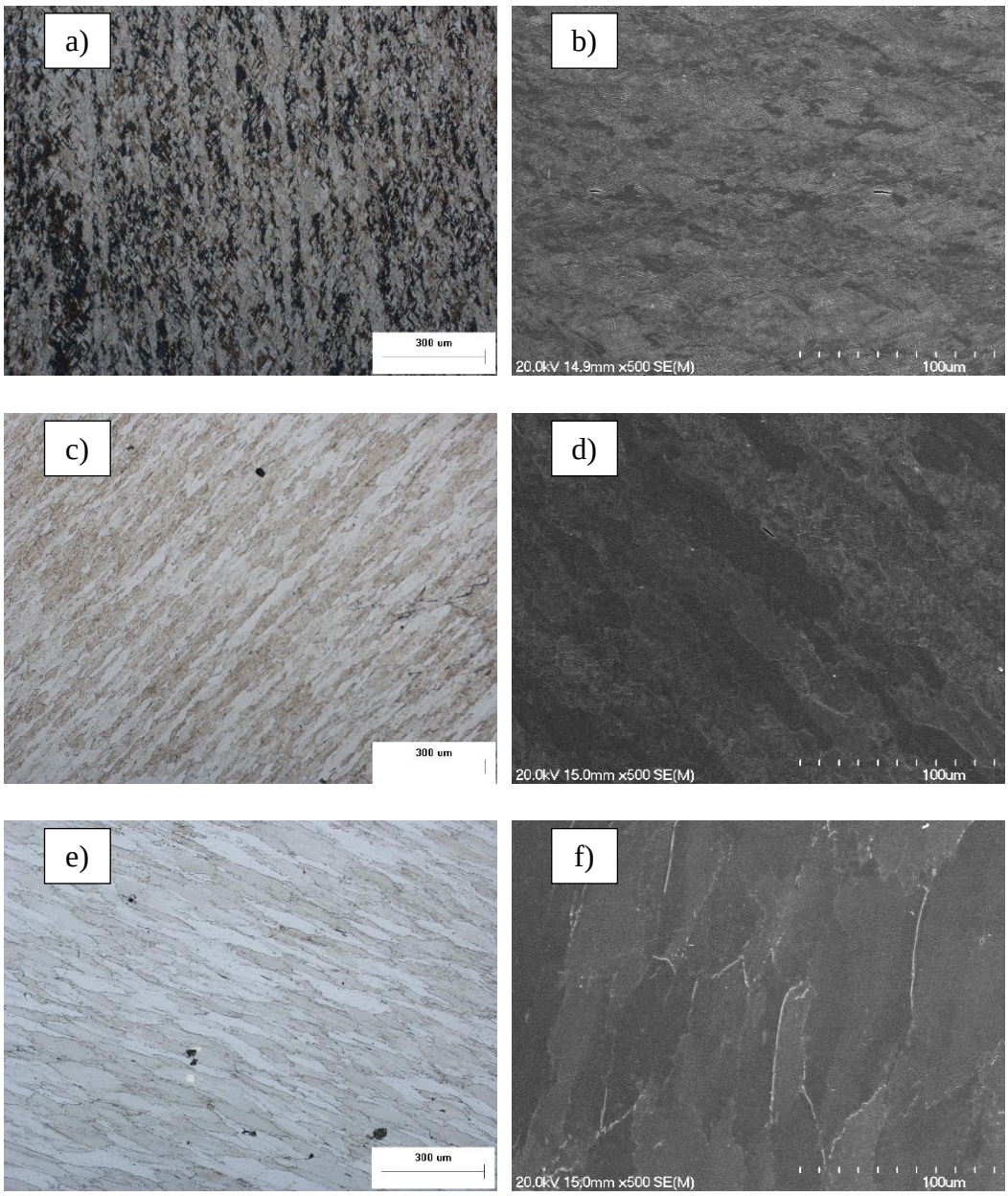

Figure 4.21 Optical micrographs and SEM images of α+β forged Ti-Mn alloys: a) and b) Ti-1Mn, c) and d) Ti-5Mn and e) and f) Ti-10Mn.

Therefore, the type of microstructure of the α+β forged and β forged materials remain the same, while the size and the shape of the porosity and of the grain is affected by the forging temperature investigated.

The results for the XRD analysis carried out on the α+β forged materials show α phase for the Ti-0.5Cu Ti-2.5Cu alloys and α and β phase plus Ti2Cu for the Ti-5Cu alloy (Figure 4.22). The results are consistent with the ones of the sintered and β forged alloys. Once again, some dissolution of the Ti_2Cu phase happens during the heating prior to forging.

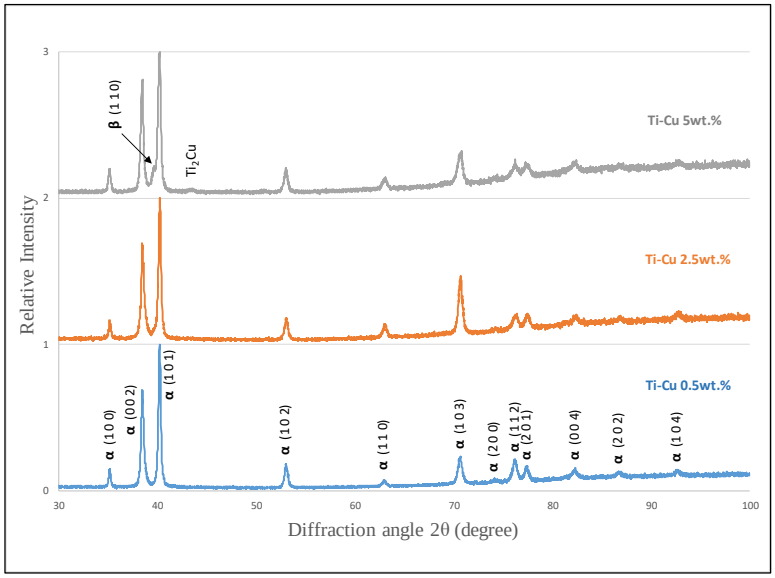

Figure 4.22 XRD patterns of the α+β forged Ti-Cu alloys.

Consistently, Figure 4.23 shows that the XRD patterns of the α+β forged Ti-Mn alloys have α phase (Ti-1Mn), and α and β phase (Ti-5Mn and Ti-10Mn alloys). The texturing effect of the forging process on the distribution of the grain of the forged mateirals is also present and it seems to be slightly more pronunced than in the case of β forging.

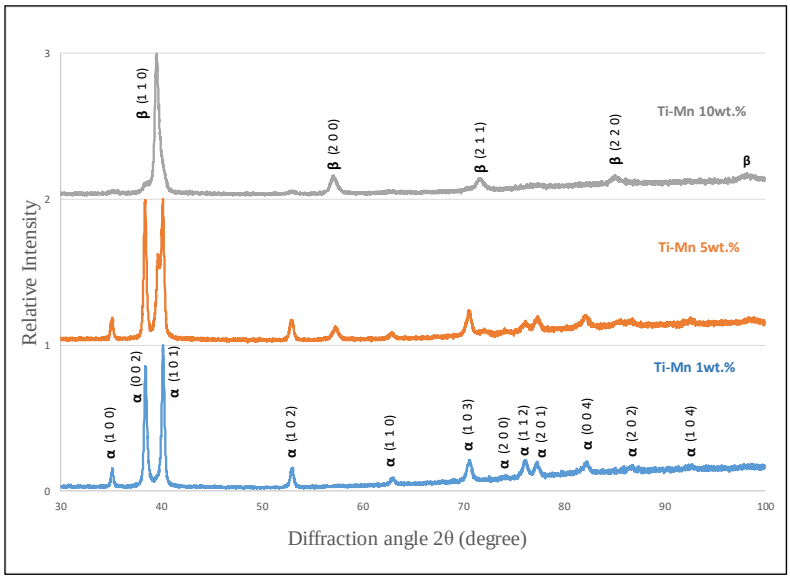

Figure 4.23 XRD patterns of the α+β forged Ti-Mn alloys.

The stress vs strain graphs of the α+β forged materials are presented in Figure 4.24 a) and b) for Ti-Cu and Ti-Mn respectively. The results show that the strength increases as the Cu and Mn content increases. Moreover, the elongation for Ti-Cu

alloys remains fairly constant, while no particular trend is found in the Ti-Mn alloys. It can be seen that the strength of the Ti-Cu and Ti-Mn alloys is higher with respect to pure Ti, but the elongation of the Ti-Cu and Ti-Mn alloys is lower.

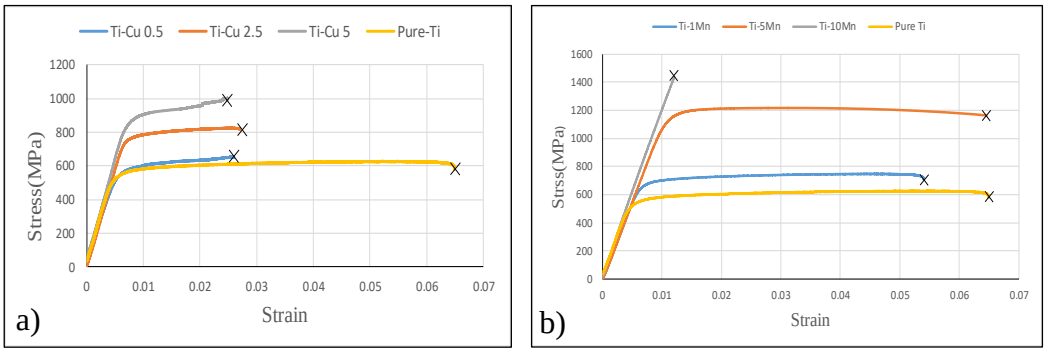

Figure 4.24 Stress-strain curves of the α+β forged d Ti-Cu (a) and Ti-Mn (b) alloys.

The variation of the average values of the strength and of the elongation with the Cu content are depicted in Figure 4.25, where a rapid increase can be seen of both UTS and YS from 647 MPa to 1035 MPa and from 572 MPa to 876 MPa respectively. Regarding the elongation, this gradually increases from 5.5% to 7%, followed by a slight decrease to 4.8% due to the presence of the Ti2Cu phase in the Ti-5Cu alloy. Likewise, there is a sharp increase in UTS from 741.33 MPa to 1442 MPa, while the YS increases from 669 MPa to 1188 MPa for the Ti-Mn alloys (Figure 4.25 b). Moreover, the elongation decreases from 10% to 1.27% due to the appearance of ω phase in the Ti-10Mn alloy.

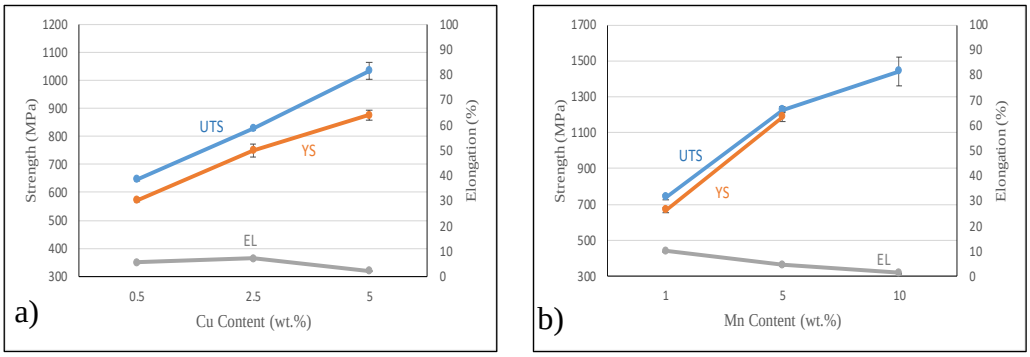

Figure 4.25 Variation of the tensile properties (UTS, YS and EL) with the amount of alloying element for α+β forged Ti-Cu (a) and Ti-Mn (b) alloys.

From the comparison of the results of the other processing routes, the α+β forged material has generally higher UTS and YS values than after sintering or β forging. Similarly, the elongation of the Ti-Cu alloys is commonly lower after α+β forged with the exception of the Ti-0.5Cu alloy processed by β forging. Conversely, in the case of the Ti-Mn alloy, the elongation is slightly higher with respect to the sintered or β forged materials.

Figure 4.26 a) and b) show the variation of the hardness of the α+β forged Ti-Cu and Ti-Mn alloys, respectively. The hardness increases along with the content of each alloying element. As the Cu content and Mn content increase the hardness increases from 238.7 to 315.3, and from 234.3 to 373.3 respectively.

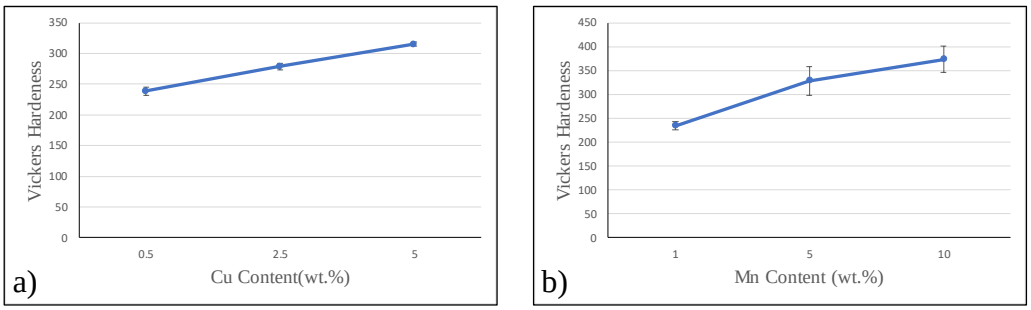

Figure 4.26 Vickers hardness of the α+β forged Ti-Cu (a) and Ti-Mn (b) alloys.

CHAPTER 5

THE UNIVERSITY OF
WAIKATO
Te Whare Wānanga o Waikato

Conclusion and recommendation

Various compositions of both Ti-Cu and Ti-Mn alloys were successfully manufactured via powder metallurgy to create fully homogeneous samples. The homogeneity was determined by EDS analysis.

Some of these samples were further hot deformed by forging where this process significantly changed the microstructural features and the mechanical properties of the different alloys. Forging is generally beneficial to reduce the amount of residual porosity, and therefore to increase the mechanical properties. However, each individual alloy has a different combination of performances as different phases in different relative ratios are present depending on the intrinsic nature of the alloy, and on the processing route used to manufacture the material.

On the basis of the characterisation performed, where the focus was on the processing and mechanical behaviour of the binary Ti-Cu and Ti-Mn alloy, it seems the Ti-5Cu and Ti-5Mn could be good candidates to test their antifouling and biofouling capabilities. The Ti-5Cu alloys can easily be manufactured via powder metallurgy, obtaining reasonable mechanical properties and should have better antifouling properties in comparison to the other Ti-Cu counterparts because of the higher Cu content and the presence of the Ti_2Cu intermetallic phase. The Ti-5Mn samples are expected to be able to contribute toward the creation of a biofilm and produce biofouling very quickly.

Suggestions for future work does not only include the determination of the antifouling and biofouling abilities, but also the quantification of the corrosion behaviour of the alloys studied as the saline environment is one of the most corrosive and disruptive for metallic structures. The effect of different heat treatments should also be investigated, as heat treatments are an easy method to change the microstructure of the alloys and thus their physical and mechanical properties, and in turn, the response once the material is submerged into a marine environment.

References

[1] D.M. Yebra, S. Kiil, K. Dam-Johansen, Antifouling technology—past, present and future steps towards efficient and environmentally friendly antifouling coatings, Progress in Organic Coatings 50(2) (2004) 75-104.

[2] A.I. Railkin, Marine biofouling: colonization processes and defenses, CRC press2003.

[3] L.D. Chambers, K.R. Stokes, F.C. Walsh, R.J.K. Wood, Corrigendum to "Modern approaches to marine antifouling coatings" [Surf. Coat. Technol. 201 (2006) 3642–3652], Surface and Coatings Technology 202(2) (2007) 412-413.

[4] M. Wahl, Marine epibiosis. I. Fouling and antifouling: some basic aspects, Marine Ecology Progress Series 58(175-189) (1989).

[5] N. Fusetani, Biofouling and antifouling, Natural Product Reports 21(1) (2004) 94-104.

[6] G. Terlinde, T. Witulski, G. Fischer, Forging of Titanium, Titanium and Titanium Alloys, Wiley-VCH Verlag GmbH & Co. KGaA2005, pp. 289-304.

[7] R. Wanhill, S. Barter, Metallurgy and Microstructure, (2012) 5-10.

[8] R.D.B. R.R. Boyer, The Use of β Titanium Alloys in the Aerospace Industry, Journal of Materials Engineering and Performance 22(10) (2013) 2916-2920.

[9] F. Zhang, A. Weidmann, J.B. Nebe, U. Beck, E. Burkel, Preparation, microstructures, mechanical properties, and cytocompatibility of TiMn alloys for biomedical applications, Journal of biomedical materials research. Part B, Applied biomaterials 94(2) (2010) 406-13.

[10] J. Gopal, P. Muraleedharan, H. Sarvamangala, R. George, R. Dayal, B. Tata, H. Khatak, K. Natarajan, Biomineralisation of manganese on titanium surfaces exposed to seawater, Biofouling 24(4) (2008) 275-282.

[11] W.-m. Guo, J.-t. Wu, F.-g. Zhang, M.-h. Zhao, Microstructure, Properties and Heat Treatment Process of Powder Metallurgy Superalloy FGH95, Journal of Iron and Steel Research, International 13(5) (2006) 65-68.

[12] S. Cao, J. Wang, H. Chen, D. Chen, Progress of marine biofouling and antifouling technologies, Chinese Science Bulletin 56(7) (2010) 598-612.

[13] G.D. Bixler, B. Bhushan, Biofouling: lessons from nature, Philos Trans A Math Phys Eng Sci 370(1967) (2012) 2381-417.

[14] M.E. Callow, J.E. Callow, Marine biofouling: a sticky problem, Biologist (London, England) 49(1) (2002) 10-4.

[15] I. Banerjee, R.C. Pangule, R.S. Kane, Antifouling coatings: recent developments in the design of surfaces that prevent fouling by proteins, bacteria, and marine organisms, Adv Mater 23(6) (2011) 690-718.

[16] L.W. H . Jacobson Sea-nine antifoulant: an environmentally acceptable

alternative to organotin antifoulants, The Science of the Total Environment 258 2000 103 Ž .]110 (2000).

[17] R.E. Baier, A.E. Meyer, Surface analysis of fouling-resistant marine coatings, Biofouling 6(2) (1992) 165-180.

[18] J.G. Burgess, K.G. Boyd, E. Armstrong, Z. Jiang, L. Yan, M. Berggren, U. May, T. Pisacane, A. Granmo, D.R. Adams, The development of a marine natural product-based antifouling paint, Biofouling 19 Suppl (2003) 197-205.

[19] P. Bhadury, P.C. Wright, Exploitation of marine algae: biogenic compounds for potential antifouling applications, Planta 219(4) (2004) 561-78.

[20] J. Liu, F. Li, C. Liu, H. Wang, B. Ren, K. Yang, E. Zhang, Effect of Cu content on the antibacterial activity of titanium-copper sintered alloys, Mater Sci Eng C Mater Biol Appl 35 (2014) 392-400.

[21] J. Gopal, P. Muraleedharan, H. Sarvamangala, R.P. George, R.K. Dayal, B.V. Tata, H.S. Khatak, K.A. Natarajan, Biomineralisation of manganese on titanium surfaces exposed to seawater, Biofouling 24(4) (2008) 275-82.

[22] B. Bai, E. Zhang, J. Liu, J. Zhu, The anti-bacterial activity of titanium-copper sintered alloy against Porphyromonas gingivalis in vitro, Dent Mater J 35(4) (2016) 659-67.

[23] L. Tamayo, M. Azocar, M. Kogan, A. Riveros, M. Paez, Copper-polymer nanocomposites: An excellent and cost-effective biocide for use on antibacterial surfaces, Mater Sci Eng C Mater Biol Appl 69 (2016) 1391-409.

[24] J.-W. Kim, M.-J. Hwang, M.-K. Han, Y.-G. Kim, H.-J. Song, Y.-J. Park, Effect of manganese on the microstructure, mechanical properties and corrosion behavior of titanium alloys, Materials Chemistry and Physics 180 (2016) 341-348.

[25] M.P. C. Leyens Titanium and Titanium alloys, 2003.

[26] M. Qian, F.H. Froes, Titanium Powder Metallurgy: Science, Technology and Applications, Elsevier, Amsterdam, Netherlands, 2015.

[27] V.A. Joshi, Titanium alloys: an atlas of structures and fracture features, Crc Press2006.

[28] M. Peters, J. Hemptenmacher, J. Kumpfert, C. Leyens, Structure and Properties of Titanium and Titanium Alloys, Titanium and Titanium Alloys, Wiley-VCH Verlag GmbH & Co. KGaA2005, pp. 1-36.

[29] T. Fujita, A. Ogawa, C. Ouchi, H. Tajima, Microstructure and properties of titanium alloy produced in the newly developed blended elemental powder metallurgy process, Materials Science and Engineering: A 213(1-2) (1996) 148-153.

[30] Q. Wang, C. Dong, P.K. Liaw, Structural Stabilities of β-Ti Alloys Studied Using a New Mo Equivalent Derived from [β/(α + β)] Phase-Boundary Slopes, Metallurgical and Materials Transactions A 46(8) (2015) 3440-3447.

[31] L. Bolzoni, P.G. Esteban, E.M. Ruiz-Navas, E. Gordo, Mechanical behaviour of pressed and sintered titanium alloys obtained from prealloyed and blended elemental powders, J Mech Behav Biomed Mater 14 (2012) 29-38.

[32] S.L. Semiatin, V. Seetharaman, I. Weiss, The thermomechanical processing of alpha/beta titanium alloys, JOM Journal of the Minerals, Metals and Materials Society 49(6) (1997) 33-39.

[33] T. Raghu, I. Balasundar, M.S. Rao, Isothermal and Near Isothermal Processing of Titanium Alloys, Defence Science Journal 61(1) (2011) 72.

[34] P. Barbosa, S. Button, Microstructure and mechanical behaviour of the isothermally forged Ti–6Al–7Nb alloy, Proceedings of the Institution of Mechanical Engineers, Part L: Journal of Materials: Design and Applications 214(1) (2000) 23-31.

[35] G. Lütjering, J.C. Williams, Titanium, Springer2003.

[36] A.K. Singh, R.A. Schwarzer, Evolution of texture during thermomechanical processing of titanium and its alloys, Transactions of the Indian Institute of Metals 61(5) (2008) 371-387.

[37] N. Gey, P. Bocher, E. Uta, L. Germain, M. Humbert, Texture and microtexture variations in a near-α titanium forged disk of bimodal microstructure, Acta Materialia 60(6–7) (2012) 2647-2655.

[38] F.C. Holden, A.A. Watts, H.R. Ogden, R.I. Jaffee, Heat Treatment and Mechanical Properties of Ti-Cu Alloys, JOM 7(1) (1955) 117-125.

[39] G. Srinivasu, Y. Natraj, A. Bhattacharjee, T.K. Nandy, G.V.S. Nageswara Rao, Tensile and fracture toughness of high strength β Titanium alloy, Ti–10V–2Fe–3Al, as a function of rolling and solution treatment temperatures, Materials & Design 47 (2013) 323-330.

[40] E. Zhang, F. Li, H. Wang, J. Liu, C. Wang, M. Li, K. Yang, A new antibacterial titanium–copper sintered alloy: preparation and antibacterial property, Materials Science and Engineering: C 33(7) (2013) 4280-4287.

[41] J. Liu, F. Li, C. Liu, H. Wang, B. Ren, K. Yang, E. Zhang, Effect of Cu content on the antibacterial activity of titanium–copper sintered alloys, Materials Science and Engineering: C 35 (2014) 392-400.

[42] E. Zhang, X. Wang, M. Chen, B. Hou, Effect of the existing form of Cu element on the mechanical properties, bio-corrosion and antibacterial properties of Ti-Cu alloys for biomedical application, Materials Science and Engineering: C 69 (2016) 1210-1221.

[43] E. Zhang, L. Zheng, J. Liu, B. Bai, C. Liu, Influence of Cu content on the cell biocompatibility of Ti–Cu sintered alloys, Materials Science and Engineering: C 46 (2015) 148-157.

[44] J. Liu, X. Zhang, H. Wang, F. Li, M. Li, K. Yang, E. Zhang, The antibacterial properties and biocompatibility of a Ti–Cu sintered alloy for biomedical application, Biomedical Materials 9(2) (2014) 025013.

[45] E. Zhang, J. Ren, S. Li, L. Yang, G. Qin, Optimization of mechanical properties, biocorrosion properties and antibacterial properties of as-cast Ti–Cu alloys, Biomedical Materials 11(6) (2016) 065001.

[46] M. Kikuchi, M. Takahashi, O. Okuno, Elastic moduli of cast Ti–Au, Ti–Ag, and Ti–Cu alloys, Dental Materials 22(7) (2006) 641-646.

[47] M. Takahashi, M. Kikuchi, Y. Takada, O. Okuno, Grindability and mechanical properties of experimental Ti–Au, Ti–Ag and Ti–Cu alloys, International Congress Series, Elsevier, 2005, pp. 326-327.

[48] M. Kikuchi, Y. Takada, S. Kiyosue, M. Yoda, M. Woldu, Z. Cai, O. Okuno, T. Okabe, Mechanical properties and microstructures of cast Ti–Cu alloys, Dental materials 19(3) (2003) 174-181.

[49] A.O. Hayama, P.N. Andrade, A. Cremasco, R.J. Contieri, C.R. Afonso, R. Caram, Effects of composition and heat treatment on the mechanical behavior of Ti–Cu alloys, Materials & Design 55 (2014) 1006-1013.

[50] S. Wang, Z. Ma, Z. Liao, J. Song, K. Yang, W. Liu, Study on improved tribological properties by alloying copper to CP-Ti and Ti–6Al–4V alloy, Materials Science and Engineering: C 57 (2015) 123-132.

[51] E. Zhang, C. Liu, Effect of surface treatments on the surface morphology, corrosion property, and antibacterial property of Ti–10Cu sintered alloy, Biomedical Materials 10(4) (2015) 045009.

[52] M.R. Akbarpour, S. Moniri Javadhesari, Wear performance of novel nanostructured Ti-Cu intermetallic alloy as a potential material for biomedical applications, Journal of Alloys and Compounds 699 (2017) 882-886.

[53] J.B. Fogagnolo, A.V. Rodrigues, E. Sallica-Leva, M.S. Lima, R. Caram, Surface stiffness gradient in Ti parts obtained by laser surface alloying with Cu and Nb, Surface and Coatings Technology 297 (2016) 34-42.

[54] C. Yongnan, H. Yazhou, Z. Yiping, S. Xuding, Z. Yongqing, B. Zhaozhao, L. Liao, Effect of Cu Content on the Semi-Solid Formability and Mechanical Properties of Ti-Cu Alloys, Rare Metal Materials and Engineering 45(6) (2016) 1406-1412.

[55] E. Zhang, S. Li, J. Ren, L. Zhang, Y. Han, Effect of extrusion processing on the microstructure, mechanical properties, biocorrosion properties and antibacterial properties of Ti-Cu sintered alloys, Materials Science and Engineering: C 69 (2016) 760-768.

[56] X. Yao, Q. Sun, L. Xiao, J. Sun, Effect of Ti 2 Cu precipitates on mechanical behavior of Ti–2.5 Cu alloy subjected to different heat treatments, Journal of Alloys and Compounds 484(1) (2009) 196-202.

[57] C. Ohkubo, I. Shimura, T. Aoki, S. Hanatani, T. Hosoi, M. Hattori, Y. Oda, T. Okabe, Wear resistance of experimental Ti–Cu alloys, Biomaterials 24(20) (2003) 3377-3381.

[58] P.F. Santos, M. Niinomi, K. Cho, M. Nakai, H. Liu, N. Ohtsu, M. Hirano, M. Ikeda, T. Narushima, Microstructures, mechanical properties and cytotoxicity of low cost beta Ti–Mn alloys for biomedical applications, Acta biomaterialia 26 (2015) 366-376.

[59] M. Shibuya, J. Nakamura, E. Akiba, Hydrogenation properties and microstructure of Ti–Mn-based alloys for hybrid hydrogen storage vessel, Journal of alloys and compounds 466(1) (2008) 558-562.

[60] A. Singh, R. Schwarzer, Effect of mode of deformation by rolling on the development of texture in binary Ti-Mn alloys, Scripta materialia 44(2) (2001) 375-380.

[61] P.F. Santos, M. Niinomi, H. Liu, K. Cho, M. Nakai, A. Trenggono, S. Champagne, H. Hermawan, T. Narushima, Improvement of microstructure, mechanical and corrosion properties of biomedical Ti-Mn alloys by Mo addition, Materials & Design 110 (2016) 414-424.

[62] X. Yu, B. Xia, Z. Wu, N. Xu, Phase structure and hydrogen sorption performance of Ti–Mn-based alloys, Materials Science and Engineering: A 373(1) (2004) 303-308.

[63] K. Cho, M. Niinomi, M. Nakai, H. Liu, P.F. Santos, Y. Itoh, M. Ikeda, T. Narushima, Improvement in mechanical strength of low-cost β-type Ti–Mn alloys fabricated by metal injection molding through cold rolling, Journal of Alloys and Compounds 664 (2016) 272-283.

[64] P.F. Santos, M. Niinomi, H. Liu, K. Cho, M. Nakai, Y. Itoh, T. Narushima, M. Ikeda, Fabrication of low-cost beta-type Ti–Mn alloys for biomedical applications by metal injection molding process and their mechanical properties, Journal of the mechanical behavior of biomedical materials 59 (2016) 497-507.

[65] A. Ibrahim, F. Zhang, E. Otterstein, E. Burkel, Processing of porous Ti and Ti5Mn foams by spark plasma sintering, Materials & Design 32(1) (2011) 146-153.

[66] B. Sharma, S.K. Vajpai, K. Ameyama, Microstructure and properties of beta Ti–Nb alloy prepared by powder metallurgy route using titanium hydride powder, Journal of Alloys and Compounds 656 (2016) 978-986.